Island Arc

Research Article

Geochemistry of eclogite- and blueschist-facies rocks from the Bantimala Complex, South Sulawesi, Indonesia: Protolith origin and tectonic setting

ADI MAULANA,[1,2,3]* ANDREW G. CHRISTY,[1,4] DAVID J. ELLIS,[1] AKIRA IMAI,[5] AND KOICHIRO WATANABE[3]

[1]*Research School of Earth Sciences, Australian National University, Canberra ACT 0200, Australia,* [2]*Department of Geology, Faculty of Engineering, Hasanuddin University, Makassar 90245, South Sulawesi, Indonesia, (email: adi-maulana@unhas.ac.id),* [3]*Department of Earth Resources Engineering, Graduate School of Engineering, Kyushu University 744 Motooka Nishi-ku, Fukuoka 819-0395, Japan,* [4]*Centre for Advanced Microscopy, Australian National University, Canberra, ACT 0200, Australia, and* [5]*Department of Earth Science and Technology, Akita University, Akita 010-8502, Japan*

Abstract We present the first data on bulk-rock major and trace element compositions for a suite of eclogite- and blueschist-facies rocks from the Bantimala Complex, Indonesia, with the aim of better constraining the protolith origins and nature of the subducted crust. The eclogites can be classified into two groups: glaucophane-rich eclogite and glaucophane-free eclogite, whereas the blueschists are divided into albite–epidote glaucophanite and quartz–glaucophane schists. SiO_2 contents of the eclogites are 43.3–49.6 wt%, with $Na_2O + K_2O$ contents 3.7–4.7 wt%. The blueschists show a wider range of compositions, with SiO_2 = 40.7–63.8 wt% and $Na_2O + K_2O$ = 2.7–4.5 wt%. Trace element data suggest that the eclogite protoliths include both enriched and normal mid-oceanic ridge basalt (E-MORB and N-MORB) and also gabbroic cumulates. The blueschists show more variation in protoliths, which include N-MORB, Oceanic Island Basalt (OIB) and Island Arc Basalt (IAB). Plots of element concentrations against the immobile Zr show considerable mobility of large ion lithophiles but not of high field-strength elements during high-pressure metamorphism, and indicate that the high SiO_2 content of some blueschists is probably due to metasomatism by a LILE-rich siliceous aqueous fluid. Strong correlations between K, Rb, Ba and Cs suggests that enrichment of these elements occurred by a single process. All the protoliths were subducted, metamorphosed to blueschist/eclogite-facies and subsequently exhumed. It is noteworthy that the samples deduced to have come from thicker-crust environments (OIB, IAB) were subducted to shallower depths (blueschist-facies) than MORB-derived samples, all except one of which reached eclogite-facies conditions. The geochemical data of this study demonstrate the variety of ocean floor types that were subducted under the southeast margin of Sundaland in the late Jurassic period.

Key words: Bantimala, blueschist, eclogite, geochemistry, Indonesia, Sulawesi.

INTRODUCTION

Plate tectonic processes have generated considerable geological complexity in Sulawesi, the four-armed island in the centre of the Indonesian Archipelago. This region shows evidence of plate convergence involving subduction of an oceanic plate (Katili 1978; Hamilton 1979; Wakita *et al.* 1996), continent–continent collision (Bergman *et al.* 1996), arc–continent collision (Elburg *et al.* 2002), sediment accretion and emplacement of dismembered ophiolites (Villeneuve *et al.* 2002; Kadarusman *et al.* 2004) and exhumation of high

and ultra-high pressure metamorphic rocks (Parkinson 1996; Wakita 2000).

The convergence of three major plates (the Eurasian, the Indian-Australian and the Pacific) has driven formation of the Sulawesi terrane complex. The westernmost parts of Sulawesi formed the eastern margin of Southeast Asia ('Sundaland') during the Mesozoic, and the rest of the island was accreted onto these, mainly in the Oligocene and Miocene (Katili 1978; Hamilton 1979; Parkinson *et al*. 1998; Charlton 2000; Villeneuve *et al*. 2002). The Cenozoic collision(s) of continental fragments have disrupted or buried much of the Mesozoic continental margin, but fragments of pre-Cenozoic basement are preserved in Sulawesi, particularly in the Bantimala Complex (Hamilton 1979; Sukamto 1982; Parkinson 1998; Parkinson *et al*. 1998; Wakita 2000; Maulana 2009).

The Bantimala Complex consists of two separate blocks: namely the Bantimala Block in the south and the Barru Block in the north (Maulana 2009). A wide variety of lithologies of various ages (Sukamto 1975; Hamilton 1979; van Leeuwen 1981; Miyazaki *et al*. 1996; Wakita *et al*. 1996; Wilson & Bosence 1996; Parkinson *et al*. 1998; Parkinson & Katayama 1999), paleogeographic anomalies (Haile 1978; Sasajima *et al*. 1980) as well as the regional structure (Berry & Grady 1987) have been reported. The basement complex contains high-pressure (blueschist, eclogite) and lower-pressure, medium-temperature (amphibolite) metamorphic rocks, as well as almost unmetamorphosed deep-marine sedimentary rocks and serpentinized ultramafics of ophiolitic affinity (Wakita *et al*. 1996; Parkinson *et al*. 1998).

The high-*P* eclogites and blueschists from this complex are of particular interest since they provide insight into the subduction zone that was operating at the eastern margin of Sundaland in the Late Mesozoic. There is much work published on the stratigraphy and structure of the complex, as cited above. However, details of the protoliths of the high-*P* rocks and their history remain uncertain (van Leeuwen 1981; Guntoro 1999). No detailed geochemical data has been reported on these rocks, to date, despite their potential to provide an important record of pressure-temperature conditions in the subduction zone, the chemistry of the subducted rocks, and hence, the tectonic settings from which their protoliths were derived. This study begins to fill that gap in knowledge, and hence contributes to our understanding of the evolution of the Indonesian Archipelago.

Trace element variation and chemical discrimination diagrams have been used in order to characterize the magma type and tectonic setting of the high-pressure metamorphic rocks. Examples of the applications of such diagrams are provided by studies such as those of Pearce and Cann (1973), Tribuzio *et al*. (1996), Winchester and Floyd (1976), Morrison (1978), Vermeesch (2006) and Van Westrenen *et al*. (2001). In using the geochemical data in this manner, we bear in mind that elemental compositions of subducted and metamorphosed igneous rocks may not be the same as those of fresh igneous rocks for a number of reasons, such as: (i) chemical alteration on the sea floor before subduction (for example addition of Na and Sr from sea water); (ii) alteration during subduction by migrating aqueous fluids; (iii) layer-parallel translation and juxtaposition of unrelated rock units to produce a rock that does not correspond to a single igneous composition, but is a tectonic mechanical mixture; and (iv) analytical error due to small and unrepresentative analytical volume (particularly in the case of rocks containing large porphyroblasts).

This report is primarily concerned with the geochemistry of the eclogite- and blueschist-facies rocks in the Bantimala Complex. We present for the first time bulk-rock, trace elements, and rare earth elements analyses of these rocks and discuss the origin of the protoliths as well as tectonic implications.

GEOLOGICAL SETTING

Sulawesi Island is one of the most complex islands in terms of its geological setting in the western Pacific region. This island has experienced events including high- pressure metamorphism, emplacement of oceanic crust, and long periods of magmatic activity through the Mesozoic and Paleogene. Based on the overall geological framework that has emerged from Polvé *et al*. (1997), Kadarusman *et al*. (2004), and Maulana (2009), Sulawesi can be divided into four lithotectonic provinces, namely: (i) the Western and North Sulawesi Pluto-Volcanic Arc; (ii) the Central Sulawesi Metamorphic Belt; (iii) the East Sulawesi Ophiolite Belt; and (iv) the Banggai-Sula and Tukang Besi Continental Fragments (Fig. 1a). The Bantimala Complex lies in the southern part of the West and North Pluto-Volcanic arc, more specifically in the south arm of Sulawesi, which is made up of Cretaceous and Paleogene sediments and
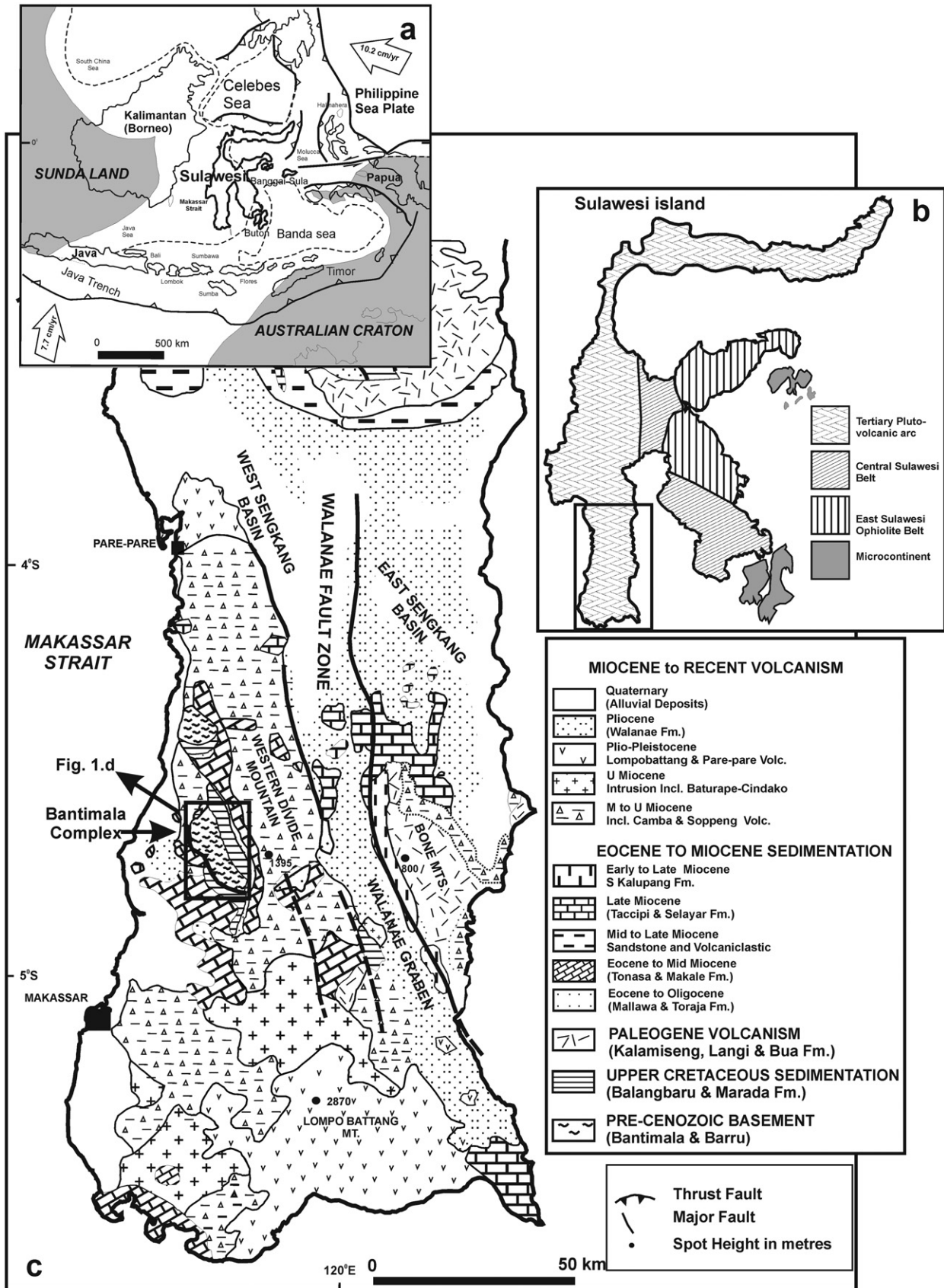
Fig. 1 (a) Plate-tectonic setting of the Indonesian Archipelago (Modified after Hamilton 1979; Hall & Wilson 2000), (b) geologic sketch map of Sulawesi, and (c) geologic map of the southern part of Sulawesi (Modified after van Leeuwen 1981).
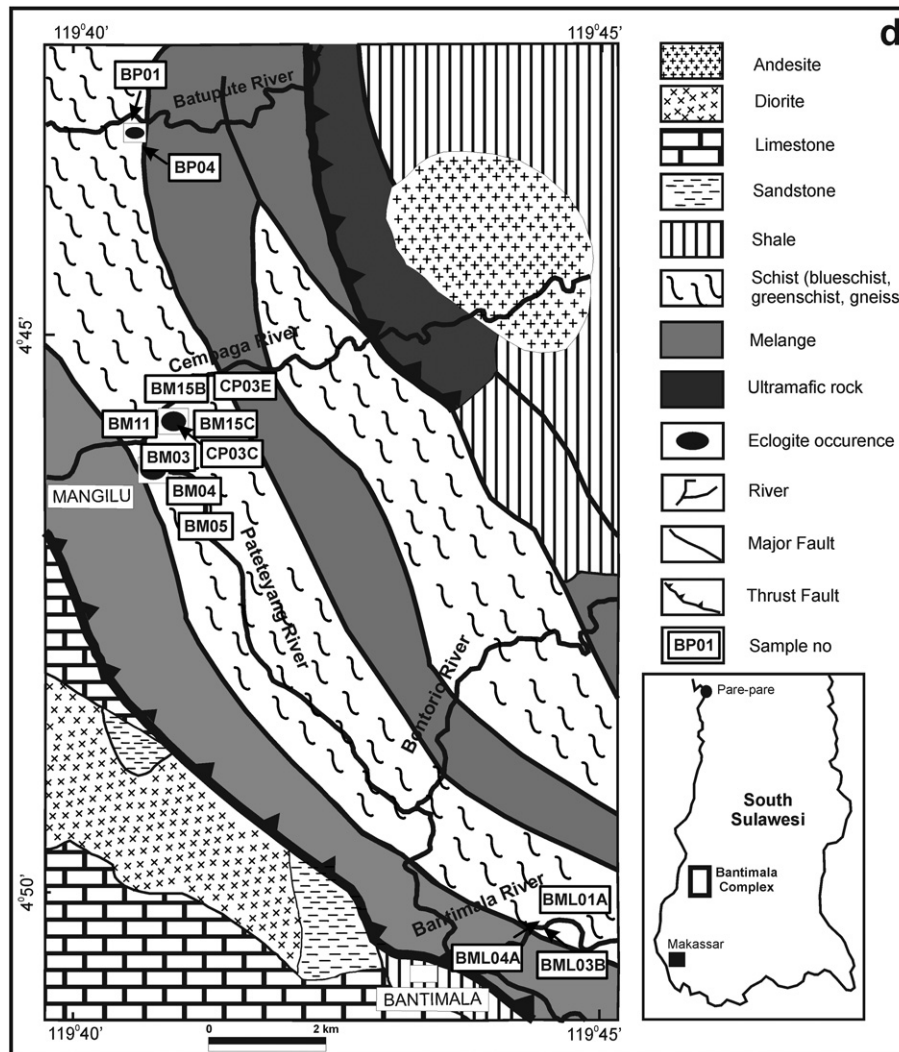
Fig. 1 *Continued* (d) Local geology of the Bantimala Complex (Maulana 2009).

volcanic arc products overlying a pre-Cenozoic basement complex. This complex was intruded in places by small igneous stocks. The detailed local geology of this complex is depicted in Figure 1b and has been discussed by Wakita *et al.* (1996) and Maulana (2009). On the basis of previous investigations, the regional geology of South Sulawesi is described as follows.

PRE-CENOZOIC BASEMENT COMPLEXES

This consists of metamorphic, sedimentary, and ultramafic rocks and occurs in two separate blocks in the Bantimala and Barru areas (Hamilton 1979; van Leeuwen 1981; Sukamto 1982). Metamorphic rocks include high-pressure types, namely glaucophane schist (Parkinson 1998), albite–actinolite–chlorite schist, chlorite–

mica schists, garnet–glaucophane rock, garnet–glaucophane–quartz schist, garnet–chloritoid–glaucophane–quartz schist (Miyazaki *et al.* 1996), quartzites, graphite phyllites (Sukamto 1982; Berry & Grady 1987), and blocks of eclogite included in blueschist (Miyazaki *et al.* 1996). The peak pressures of the Bantimala eclogites were 18–24 kbar with temperature range of 580–640°C (Miyazaki *et al.* 1996). Whole-rock ages using K–Ar dating on muscovite–garnet and quartz–muscovite schists from the Bantimala basement complex are 111 Ma (Hamilton 1979). In addition, Wakita *et al.* (1996) reported muscovite K–Ar ages of 132–113 Ma and 115–114 Ma from eclogite and greenschist-facies rocks, respectively. These suggest that an oceanic plate subducted beneath the Sundaland continent during the Late Jurassic or earliest Cretaceous (Wakita *et al.* 1996). The sedimentary

rocks are comprised of mélange, turbidite, and shallow-marine clastic rocks (Wakita *et al.* 1996). Mélange includes clasts of rock types such as sandstone, shale, siliceous shale, chert, basalt, schist, and felsic igneous rocks within a sheared matrix. The Middle Cretaceous (Late Albian–Early Cenomanian, i.e. about 105–95 Ma) chert unconformably overlies the high-pressure metamorphic rocks (Wakita *et al.* 1996). Tectonic slices also occur of Jurassic shallow-marine sedimentary rocks called the Paremba Sandstone (Sukamto 1975; Wakita *et al.* 1996): lithologies are thinly-bedded sandstone and shale intercalated with thin limestone layers in the lower part, and conglomerate containing basalt and schist pebbles in the upper part of this formation. The ultramafic rocks are dominated by serpentinized peridotite, which contains chromite lenses in some areas and is locally intruded by dacite and andesite (van Leeuwen 1981).

UPPER CRETACEOUS SEDIMENTS

These consist of three formations, namely the Balangbaru Formation, which is found in the western part of the region (Sukamto 1982), the Marada Formation (van Leeuwen 1981) confined to the Biru region, and the Latimojong Formation in the northern part of the region. The Balangbaru Formation unconformably overlies the basement complex, and is composed of interbedded sandstones and shales, with subordinate conglomerates, pebbly sandstones and conglomeratic breccias (Sukamto 1982). The Marada Formation consists of a flysch-like sequence of greywackes, arkosic sandstone and shales of Late Cretaceous age (van Leeuwen 1981). The Latimojong Formation consists of alternating beds of phylite, shale, quartzite, marble and limestone with conglomerate and chert intercalations. The thickness of this formation is more than 1 km (Simandjuntak *et al.* 1991).

PALEOGENE VOLCANICS

Paleogene volcanism in the region is represented by the Kalamiseng, Langi, and Bua Volcanics which unconformably overlie the Upper Cretaceous sediments, and in turn are unconformably overlain by Eocene sediments. The volcanics consist of lavas and pyroclastic deposits of andesitic to trachyandesitic composition, with rare intercalations of limestone and shale towards the top of the sequence (van Leeuwen 1981; Sukamto 1982). Fission-track dating of zircon from tuff at

the lower part of the volcanic sequence yielded an Early Paleocene age of 63 ± 2.2 Ma (van Leeuwen 1981), whereas K–Ar dating from biotite monzonite in the Langi Intrusion gives an age of 52.3 ± 0.5 Ma (Elburg *et al.* 2002).

EOCENE TO RECENT SEDIMENTS AND VOLCANICS

Eocene to Recent sediments and volcanics can be found throughout the southern part of Western Sulawesi. The Eocene sedimentary rocks are composed of various compositions of rocks, including claystone to conglomerates with layers or lenses of coal and limestone, various carbonate sequences and volcanic tuff, volcanic conglomerates and breccia (van Leeuwen 1981; Sukamto & Supriatna 1982; Wilson & Bosence 1996; Maryanto *et al.* 2004).

The Miocene to Recent volcanic rocks consist of various formations and are widely distributed surrounding the Bantimala Complex, including, in order of decreasing age, the Upper Camba Formation, Baturape–Cindako Volcanics, Soppeng Volcanics, Parepare Volcanics, Lemo Volcanics, and the Lompobattang Volcanics (van Leeuwen 1981; Sukamto 1982; Sukamto & Supriatna 1982; Yuwono *et al.* 1988; Leterrier *et al.* 1990; Polvé *et al.* 1997; Elburg *et al.* 2002). The sedimentary rocks are made up of a volcanic series interbedded with marine sediments, whereas the volcanic rocks consist of a basaltic flow and alternating lava flows (dominated by basaltic in composition) and pyroclastic breccias. In addition, rhyolite blocks, dacite, volcanic breccia, tuff, lava, and dikes more than 350 m in thickness were reported.

SAMPLE DESCRIPTIONS AND ANALYTICAL METHODS

Thirteen samples of high-pressure rocks, six eclogites, and seven blueschists were analyzed. All samples were studied petrographically to determine the rock types, mineral assemblages, fabric, and textural relations. Modal compositions of the samples are given in Table 1.

The eclogites occur as tectonic blocks within blueschist units, typically several metres across, and often show vestiges of pillow lava structure as shown in Figure 2a and b. In addition to garnet + omphacite + quartz + phengite ± epidote ± glaucophane + rutile as primary phases, many of these eclogites contain chlorite and/or actinolite.

Table 1 Modal abundances (in vol.%) of minerals in eclogites and blueschists from the Bantimala Complex

Locality	Rock-type	Sample number	Garnet	Omphacite	Glaucophane	Phengite	Epidote	Quartz	Titanite	Rutile	Apatite	Albite	Zircon	Alt†
Cempaga	Glaucophane-rich eclogite	BM11	30–35	35–40	5	7–9	5–7	2–3	1	1	1	–	+	3
Cempaga		BM15B	42–45	32–36	6–8	3–5	6	–	<1	1	1	–	+	3
Batupute		BP04	40–42	30–35	8–10	5	4–6	1	1	1	1	–	–	2
Cempaga		CP03E	38–40	32–35	6–8; Bar: 3	12–15	2	<1	1	2	<1	–	–	2
Batupute	Glaucophane-free eclogite	BP01	36	42–44	–	10–12	13–15	2	1	2–3	1	–	–	2
Bantimala		BM15C	30–34	38–40	–	10–11	10–12	1	1	2–4	<1	<1	–	3
Pateteyang	Albite–epidote glaucophanite	BM03	–	–	72–75	5–8	5–7	2	1	<1	<1	10–12	+	2
Pateteyang		BM04	5	2	70–76	–	5–8	<2	1	2	1	7–9	+	2
Bantimala		BML01A	–	–	74–78	3–6	8–11	2	1	–	1–2	13–15	+	2
Bantimala		BML04A	–	–	72–78	6–8	8–10	2	–	–	–	6–8	–	3
Pateteyang	Quartz glaucophane schist	BM05	6	–	45–50	10–15	6–8	22–25	1	1	–	2	–	3
Bantimala		BML03B	5	–	50–52	12–14	6–8	20–25	–	–	–	–	–	3
Cempaga		CP03C	4	–	50–55	10–12	5–7	26–30	–	–	–	1	–	1

Alt†, alteration (chlorite, magnetite, ilmenite); Bar, Barroisite; Act, actinolite; +, abundance.

Apatite occurs in all samples except BP01. On the basis of mineralogy, the eclogites can be divided into two types: glaucophane-rich eclogite and glaucophane-free eclogite. Glaucophane-rich eclogite is found as either tectonic blocks within the blueschist, or as cobbles and boulders along the rivers. The rock is mainly composed of garnet + omphacite + glaucophane + phengite + epidote + quartz + rutile, with zircon, titanite, and opaque oxide as accessory minerals. Garnet occurs as porphyroblasts (up to 5 mm in diameter) set in omphacite and phengite, as well as in glaucophane matrix (Fig. 2c). Glaucophane-free eclogite is dark green to greyish green in colour, with patchily distributed red-brown garnet porphyroblasts. It is composed of garnet + omphacite + epidote + phengite + quartz + rutile with accessory zircon, titanite, apatite, calcite, and opaque oxide. Garnet ranges from euhedral to strongly resorbed, chloritized, and fractured, with porphyroblasts up to 6 mm in size. They contain numerous randomly oriented inclusions in their central portions as well as the outer rims, and are sometimes surrounded by complex reaction rims of retrograde chlorite and albite in BM15C (Fig. 2d).

Blueschist-facies rocks are distinguished from eclogites by the absence of omphacite in the matrix. They are composed mainly of glaucophane with garnet or albite and other minerals, but without omphacite except in BM04, where omphacite occurs as inclusions in garnet, suggesting blueschist-facies overprinting of an earlier eclogite assemblage. They are often characterized by alteration of garnet and glaucophane to form chlorite. Based on mineral assemblages, two major types of blueschist were identified: albite–epidote–glaucophanite and quartz–glaucophane schist. The albite–epidote–glaucophanite has a massive fabric, lacking foliation, and is essentially composed of garnet porphyroblasts that have been strongly chloritized (Fig. 2e) in a medium- to fine-grained matrix of glaucophane/actinolite (up to 78 vol.%), albite, epidote, phengite, chlorite, quartz and titanite with rutile, ilmenite, apatite, pyrite, chalcopyrite, zoisite, and tiny zircons as accessory minerals. The quartz–glaucophane schist is characterized by a good foliation, defined by orientation of quartz, blue amphibole and micas (Fig. 2f). The rocks consist of quartz, glaucophane, garnet, chlorite, phengite, albite, and epidote. Rutile is present as an accessory mineral and is sometimes armoured by titanite.

Quantitative compositional data for the minerals were obtained using a JEOL 6400 scanning
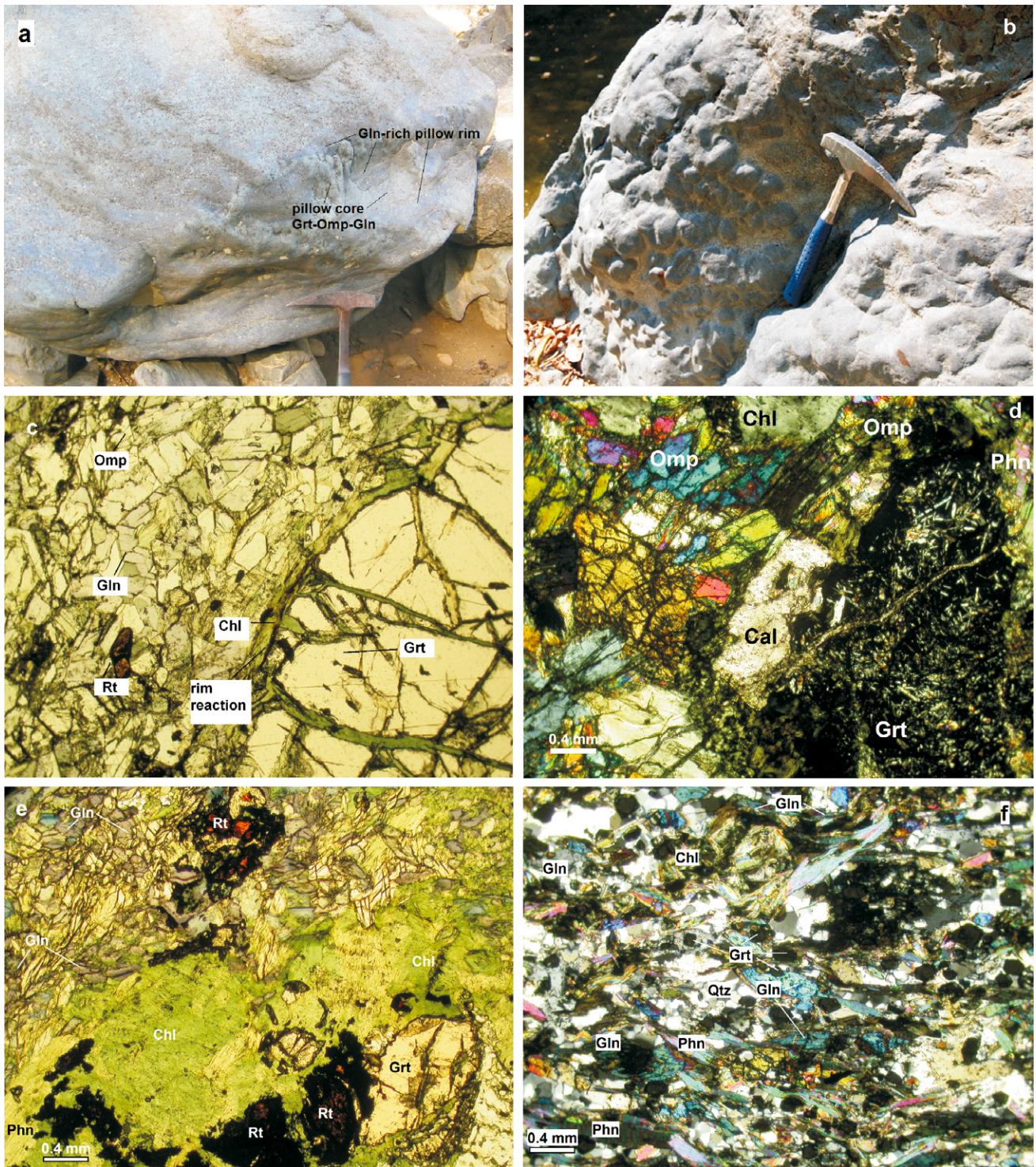
Fig. 2 (a) Field photograph of eclogite in Pateteyang River, showing pillow lava structure. Pillow cores contain garnet (Grt) + omphacite (Omp) + epidote (Ep) + glaucophane (Gln) with glaucophane (Gln) - rich pillow rim. (b) Pillow lava structure shown by eclogite outcrop in Cempaga River. (c) Garnet porphyroblast in glaucophane and omphacite matrix (CP03E) with plane polarized light. (d) Garnet containing numerous randomly oriented inclusions surrounded by chlorite and albite + omphacite symplectite in BM15C with crossed polars. (e) Albite epidote glaucophanite (sample BM04) showing chloritiszed garnet porphyroblast and rutile set in glaucophane matrix (plane-polarized light). (f) Glaucophane (Gln), phengite (Phn) and chlorite (Chl) define the foliation in a groundmass of quartz grains in BML03B (crossed polars).

electron microscope, equipped with an Oxford Instruments energy-dispersive spectrometer (EDS) detector and Link ISIS analytical software. Operating conditions for the energy-dispersive X-ray analyses (EDXA) were 15 kV accelerating voltage, 1 nA beam current, and a range of beam diameters (focused beam for garnet; beam defocused to 5 μm for micas and plagioclase so as to avoid alkali loss). Natural mineral standards and the ZAF matrix correction routine were used. The following standard were used: sanidine for Si and K, albite for Na and Al, diopside for Ca, TiO_2 and pure Ti for Ti, Fe_2O_3 for Fe, Cr_2O_3 for Cr, MgO for Mg, pure Mn for Mn, pure apatite for P, zircon for Zr and Hf, calcite for Ca, pyrite for S, chalcopyrite for Cu, pure Co for Co, pure nickel for Ni, and baryte for Ba. All samples were polished with 1 μm diamond paste and carbon coated to approximately 20 nm thickness. In addition to spot analyses, the SEM was used to construct X-ray maps for Fe, Mn, Mg, Ca, and either Al or Si by using a beam current of 100 nA, 50 ms dwell time, and 5–9 mm scanned area. These facilitated the identification of minerals in back-scattered electron images, and the location of uncommon accessory minerals. SEM analyses and carbon coating were carried out at the Electron Microscopy Unit (now the Centre for Advanced Microscopy) at ANU, Canberra.

The samples were crushed and milled to obtain homogeneous powders for whole-rock analyses. Bulk-rock major elements were analyzed by X-ray fluorescence analysis (XRF), and whole-rock and individual mineral trace element were analyzed by laser ablation inductively-coupled plasma mass spectrometry (LA–ICP–MS). Na, Mg, Al, Si, P, S, K, Ca, Ti, Mn, and Fe, plus F and Cl were analyzed using a Phillips PW2400 wavelength-dispersive XRF spectrometer at the Research School of Earth Sciences, ANU. Lithium borate discs were prepared by fusion of 0.27 g of dried sample powder with 1.72 g of '12–22' eutectic $LiBO_2$–$Li_2B_4O_7$ at 1010°C for 10 min in a rocker furnace. The XRF spectrometer was calibrated for major elements against a set of 28 international standard rock powders.

Trace element analyses were obtained by LA–ICP–MS at the Research School of Earth Sciences, ANU. Trace elements concentrations were determined on glass beads made from rock powders fused with lithium borate flux (1: 3 mass ratio). The LA–ICP–MS employs an ArF^+ (193 nm) excimer laser and a Hewlett Packard Agilent 7500 ICP-MS. Laser sampling was performed in an Ar–He atmosphere using a spot size between 80 and 100 μm. The counting time was 20 seconds for the background and 40 seconds for sample analyses. The external standard for calibration was NIST 612 glass, using the standard reference values of Pearce *et al.* (1997). Si was used as the internal standard, employing the SiO_2 concentration previously measured by XRF. Relative uncertainties in the trace element analyses calculated from counting statistics were typically ± 1–2% for abundant transition metals and light rare earths, larger for scarce elements. Estimate standard deviations are quoted in Tables 3 and 4.

Loss on ignition (LOI) values were calculated from the mass change in approximately 2 grams of a powdered sample after heating to 1010°C in the furnace for one hour.

MINERAL CHEMISTRY

Representative microprobe analyses of garnet, clinopyroxene, amphibole, phengite, and epidote are given in Table 2. Garnet end-members were calculated according to the method of Rickwood (1968). Garnet compositions are almandine- and grossular-rich (Fig. 3a), typical of group C eclogites (Coleman *et al.* 1965). Zoning is common in garnet particularly in the eclogite-facies rocks. A profile across a typical garnet from sample BM16 showed a U-shaped profile from Mg-rich rim A ($Alm_{65.8}Prp_{13.9}Grs_{18.8}Sps_{1.4}$) to a core region low in Mg ($Alm_{64.8}Prp_{5.8}Grs_{24.1}Sps_{5.3}$) to the opposite Mg-rich rim B ($Alm_{65.4}Prp_{15.9}Grs_{17.8}Sps_{21.7}$), suggesting prograde growth (Krogh 1982). Pyroxene formulae and Fe^{2+}/Fe^{3+} ratios were calculated by normalizing the analyses to 4 cations per 6 oxygens, following the method of Ryburn *et al.* (1976). Normalized pyroxene end member components for eclogite- and blueschist-facies rocks were calculated on the basis of $X_{Jd} = Al^{VI}/(Na + Ca)$, $X_{Acm} = Fe^{3+}/(Na + Ca)$, and $X_{Aug} = (Ca)/(Na + Ca)$ (Morimoto *et al.* 1988) and plotted on the jadeite–aegirine–augite (Jd–Aeg–Aug) diagram of Essene and Fyfe (1967), as shown in Figure 3b. The Fe^{3+} and Fe^{2+} contents of the amphiboles were estimated on the assumptions that Si + Al + Ti + Cr + Fe + Mn + Mg = 13, and 23 oxygens were needed for charge balance (Droop 1987). Amphiboles were named following the classification of Leake *et al.* (1997, 2003). The compositional range of amphibole is shown in Figure 3c, as a function of Na (B-site) *vs* Si content in formula.

Table 2 Selected microprobe analyses of eclogite and blueschist minerals from the Bantimala Complex

Mineral	Garnet				Omphacite				Glaucophane				Phengite				Epidote			
Sample no	BM 15B		BM 03		BM 15B		BM 04		BM 15B		BM03		CP03E		BML01A		CP03E		BM 05	
Rock-type	Eclogite		Blueschist		Eclogite		Blueschist		Eclogite		Blueschist		Eclogite		Blueschist		Eclogite		Blueschist	
Location	core	rim	mtx	mtx	mtx	inc	Inc	Inc	inc	Mtx	mtx	mtx	mtx	mtx	mtx	mtx	inc	mtx	mtx	mtx
SiO$_2$	37.31	38.06	37.46	37.16	55.10	54.91	55.32	55.91	55.52	57.69	58.81	58.38	52.37	50.34	51.87	50.38	37.84	37.99	37.30	37.20
TiO$_2$	0.00	0.06	0.00	0.18	0.19	0.11	0.18	0.00	0.53	0.22	0.00	0.03	0.32	0.20	0.23	0.46	0.14	0.32	0.30	0.23
Al$_2$O$_3$	20.80	21.43	20.90	20.99	8.52	9.09	7.96	8.14	7.88	10.36	8.76	7.81	23.96	25.03	23.67	27.03	24.13	26.41	22.73	23.08
Cr$_2$O$_3$	0.01	0.10	0.00	0.00	0.10	0.03	0.00	0.00	0.03	0.00	0.10	0.00	0.00	0.20	0.00	0.04	0.00	0.01	0.15	0.01
FeO	31.05	27.55	28.50	28.24	9.29	10.44	11.18	10.52	19.59	7.85	13.16	13.13	2.08	2.83	3.78	3.72	11.41	9.55	12.52	12.26
MnO	0.52	0.55	1.45	1.39	0.00	0.04	0.05	0.09	0.08	0.11	0.15	0.05	0.05	0.00	0.02	0.06	0.32	0.18	0.08	0.33
MgO	3.44	5.92	3.68	3.83	6.74	6.36	6.88	6.14	5.63	12.37	10.56	11.29	4.68	4.19	4.29	3.41	0.06	0.54	0.00	0.09
CaO	7.05	6.91	8.16	8.43	11.82	11.65	12.25	11.72	0.92	1.25	0.65	1.58	0.00	0.00	0.02	0.00	23.40	21.64	23.16	23.26
Na$_2$O	0.18	0.17	0.00	0.19	7.37	7.50	6.92	7.58	6.32	6.65	7.13	6.56	0.00	0.00	0.24	0.52	0.02	0.23	0.00	0.06
K$_2$O	0.00	0.00	0.00	0.00	0.00	0.00	0.00	0.00	0.00	0.00	0.00	0.00	10.67	10.67	10.69	10.33	0.00	0.03	0.05	0.00
Total	100.36	100.75	100.15	100.41	99.13	100.13	100.74	100.10	96.50	96.50	99.32	98.83	94.13	93.46	94.81	95.95	97.32	96.90	96.29	96.52
Si	2.97	2.96	2.97	2.94	2.00	2.00	2.00	2.00	7.99	7.88	7.96	7.95	3.53	3.44	3.51	3.37	2.99	2.98	2.99	2.97
Al tet	0.03	0.04	0.03	0.06	0.00	0.00	0.00	0.00	0.01	0.12	0.04	0.05	0.47	0.56	0.49	0.63	0.01	0.02	0.01	0.03
Al oct	1.92	1.93	1.93	1.91	0.36	0.39	0.34	0.34	1.39	1.55	1.35	1.20	1.44	1.46	1.40	1.50	2.23	2.42	2.13	2.15
Ti	0.00	0.00	0.00	0.01	0.01	0.00	0.00	0.00	0.06	0.02	0.00	0.00	0.02	0.01	0.01	0.02	0.01	0.02	0.02	0.01
Cr	0.00	0.01	0.00	0.00	0.00	0.00	0.00	0.00	0.00	0.00	0.01	0.00	0.00	0.01	0.00	0.00	0.00	0.00	0.01	0.00
Fe^{3+}	0.00	0.00	0.00	0.00	0.15	0.05	0.11	0.26	0.00	0.40	0.63	0.64	0.00	0.00	0.00	0.00	0.75	0.63	0.84	0.82
Fe^{2+}	2.07	1.79	1.89	1.87	0.13	0.27	0.23	0.06	2.46	0.50	0.86	0.85	0.12	0.16	0.21	0.21	0.00	0.01	0.00	0.00
Mn	0.04	0.04	0.10	0.09	0.00	0.00	0.00	0.00	0.01	0.01	0.02	0.01	0.00	0.00	0.00	0.00	0.02	0.01	0.01	0.00
Mg	0.41	0.69	0.44	0.45	0.36	0.35	0.37	0.33	1.26	2.52	2.13	2.29	0.47	0.43	0.43	0.34	0.01	0.06	0.00	0.01
Ca	0.60	0.58	0.69	0.72	0.46	0.45	0.47	0.45	0.15	0.18	0.09	0.23	0.00	0.00	0.00	0.00	1.98	1.82	1.99	1.99
Na	0.03	0.00	0.00	0.03	0.52	0.53	0.49	0.53	1.84	1.76	1.87	1.73	0.00	0.00	0.03	0.07	0.00	0.03	0.00	0.00
K	0.00	0.00	0.00	0.00	0.00	0.00	0.00	0.00	0.00	0.00	0.00	0.00	0.92	0.93	0.92	0.88	0.00	0.00	0.01	0.00
Total	8.07	8.03	8.05	8.08	4.00	4.04	4.0	4.0	15.17	14.94	14.96	14.96	6.96	7.00	7.01	7.02	8.01	7.99	8.00	8.02

Garnet formulae normalized to 8 cations and 12 oxygens; omphacite to 4 cations and 6 oxygens; glaucophane to 23 oxygens; phengite to 11 oxygens and epidote to 12.5 oxygens.
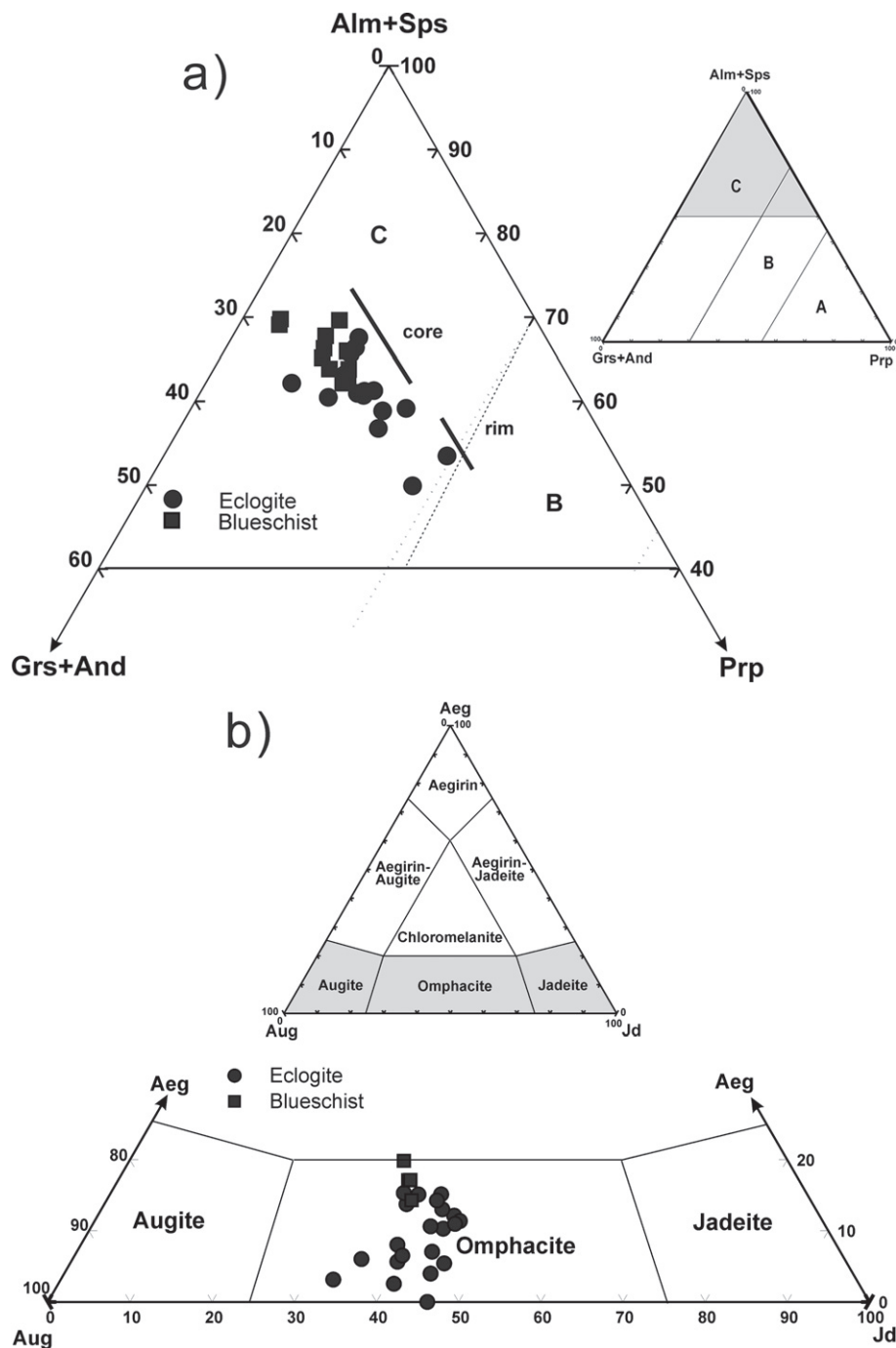
Fig. 3 (a) Garnet compositions from eclogite and blueschist in the Bantimala Complex plotted in the diagram of Coleman *et al.* (1965). (b) Clinopyroxene compositions of the eclogite and blueschist rocks plotted in Aug-Aeg-Jd diagram of Essene and Fyfe (1967). (c) Amphibole compositions plotted on a diagram of Na (B-site) *vs* Si (cf. Leake *et al.* 1997, 2003). (d) Mica compositions plotted in Si *vs* Al (atomic per formula unit) diagram.

Analyzed sodic (Na) amphiboles fall into the glaucophane–magnesioriebeckite field, particularly those from blueschist-facies rock. Calcic (Ca) amphibole lies in the actinolite–tremolite field, whereas (Na–Ca) amphibole is winchite–barroisite.

Mica formulae were calculated to 11 oxygens, assuming all iron to be Fe^{2+}. Mica-group minerals

are phengite and paragonite (Fig. 3d). Phengite is present in all analyzed samples, whereas paragonite only occurs in the eclogite BP01 and blueschist BML04A. Si contents of phengite in eclogite are 3.38–3.53 atoms per formula unit (a.p.f.u.), whereas those in blueschist overlap the lower part of this range. This high Si content indicates crystallization at high pressure (Carswell *et al.*
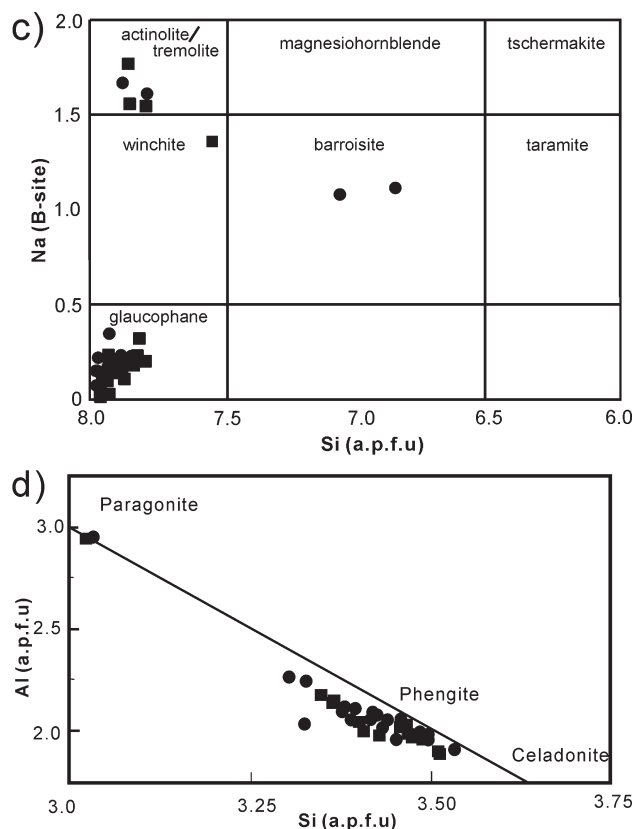
Fig. 3 *Continued*

1997). However, Si as low as 3.23 a.p.f.u. is found for phengite replacing omphacite in garnet from eclogite CP03E, suggesting lower pressure for this texturally late phengite.

Epidote group formulae were calculated to 12.5 oxygens, assuming all iron to be Fe^{3+}. Epidotes in eclogite and blueschist yield similar $X_{Ps} = Fe^{3+}$ p.f.u values of 0.63–0.75 and 0.82–0.84, respectively. Generally, epidote in the matrix shows lower Fe^{3+} than epidote inclusions.

GEOCHEMISTRY

BULK ROCKS

Compositional data for the eclogite- and blueschist-facies rocks from the Bantimala Complex are shown in Tables 3 and 4, respectively. The eclogites were characterized by low SiO_2 content (45.3 to 49.6 wt%), whereas K_2O ranges from 0.03 to 1.36 wt%, and Na_2O ranges from 2.6 to 3.9 wt%. For initial descriptive purposes, we plotted bulk compositions in the Total Alkali *vs* Silica (TAS) and Al_2O_3–FeO–MgO (AFM) diagrams typically used for mafic rocks. We note that

contents of some of the relevant chemical components are likely to have been perturbed by seafloor alteration or subsequent metamorphism, and indeed show evidence of such mobility later. Hence, the current position of rocks in such diagrams should not be interpreted as similar to the protolith position without caution. In the TAS diagram (Fig. 4a), all samples fall in the basalt field, while on an AFM diagram, samples all appear to lie along an Fe-enrichment trend which is consistent with tholeiitic rather than calc-alkaline affinity (Fig. 4b). The wide range of Mg number $(100MgO/(MgO + FeO_{Total}) = 37.6–64.4)$ indicates a range of igneous fractionation. The analyzed blueschists are characterized by high variation in SiO_2 and total alkali concentrations, correlating with the mineral assemblage and possible protolith sources, and reflecting change in the contents of mobile components SiO_2, Na_2O and K_2O from their original igneous values. The albite–epidote–glaucophanites mostly plot in the basalt field in the TAS diagram (Fig. 4a) with the exception of sample BM04 (picrobasalt field), while the quartz–glaucophane schists are characterized by high SiO_2 (58 to 63 wt%) and all plotted in the

Table 3 Whole-rock and trace elements compositions of eclogites from the Bantimala Complex, South Sulawesi

Sample	BM11	BM15B	BP04	CP03E	BP01	BM15C
Rock-type		Glaucophane-rich eclogite			Glaucophane-free eclogite	
Whole-rock (wt%)						
SiO_2	47.30	45.32	49.61	46.60	45.87	46.24
TiO_2	1.70	4.56	1.43	0.49	0.46	0.83
Al_2O_3	14.76	14.05	14.88	16.85	16.66	12.65
FeO_{Tot}	10.92	16.55	12.11	15.33	9.02	11.10
MnO	0.18	0.29	0.24	0.67	0.29	0.34
MgO	7.67	5.61	7.30	7.70	8.30	11.28
CaO	11.77	10.56	6.58	8.92	13.27	10.49
Na_2O	3.93	3.69	2.87	2.61	3.73	3.92
K_2O	0.74	0.03	1.02	1.36	0.19	0.14
P_2O_5	0.05	0.16	0.08	0.11	0.01	0.01
SO_3	nd	nd	nd	nd	Nd	nd
F	0.06	nd	0.04	0.10	0.03	nd
Cl	nd	nd	nd	nd	Nd	nd
$-O \equiv F$	−0.03	–	−0.02	−0.04	−0.01	–
$-O \equiv Cl$	–	–	–	–	–	–
LOI	1.79	0.01	3.48	0.08	3.12	3.60
Total	100.84	100.82	99.64	100.78	100.94	100.58
Trace elements (µg/g)						
Be	1.12 (8)	1.34 (8)	0.51 (5)	0.93 (6)	0.43 (4)	1.73 (9)
Sc	42.8 (5)	54.9 (7)	50.2 (6)	60.3 (7)	39.1 (5)	39.0 (5)
V	289 (2)	452 (4)	329 (3)	272 (2)	217 (2)	355 (3)
Cr	299 (5)	123 (2)	141 (2)	56.2 (13)	46.2 (10)	630 (9)
Ni	61.8 (13)	42.2 (13)	48.5 (18)	39.1 (10)	70 (3)	222 (10)
Cu	123 (2)	26.8 (5)	53.8 (8)	9.3 (3)	14.3 (3)	7.9 (2)
Zn	45.6 (8)	74.9 (10)	73.2 (11)	58.1 (9)	91.3 (13)	38.6 (7)
Ga	15.6 (3)	16.9 (3)	14.0 (2)	11.2 (2)	14.2 (2)	11.4 (2)
Ge	2.4 (2)	3.2 (2)	1.7 (2)	1.8 (2)	1.45 (14)	1.86 (13)
As	0.48 (13)	0.97 (10)	0.48 (11)	0.49 (12)	0.74 (12)	0.65 (8)
Rb	18.7 (3)	1.38 (6)	17.7 (3)	31.4 (4)	3.37 (9)	3.83 (9)
Sr	666 (7)	153 (1)	206 (2)	64.4 (7)	1312 (13)	908 (10)
Y	28.4 (4)	77.0 (8)	30.1 (4)	26.8 (4)	12.6 (2)	43.1 (5)
Zr	125 (2)	343 (4)	62.5 (8)	60.2 (9)	17.0 (3)	71.4 (10)
Nb	13.5 (2)	17.7 (3)	0.89 (5)	0.62 (4)	0.57 (3)	1.28 (5)
Mo	1.09 (9)	0.91 (7)	0.61 (7)	0.69 (9)	0.49 (5)	0.88 (7)
Ag	0.25 (3)	0.30 (3)	0.23 (3)	0.10 (2)	0.20 (2)	0.26 (3)
Cd	0.19 (9)	0.31 (10)	0.17 (2)	0.28 (11)	<0.2	0.17 (6)
In	0.20 (2)	0.14 (2)	0.15 (2)	0.11 (2)	0.03 (1)	0.03 (1)
Sn	29.7 (5)	3.3 (2)	20.1 (5)	1.61 (12)	0.52 (6)	0.44 (5)
Sb	3.0 (2)	3.1 (2)	2.86 (12)	3.00 (14)	2.76 (12)	2.36 (10)
Cs	0.42 (4)	0.11 (2)	0.37 (3)	1.93 (8)	0.26 (3)	0.22 (2)
Ba	148 (2)	16.3 (3)	129 (2)	185 (2)	96.7 (12)	82.2 (11)
La	12.3 (3)	16.0 (3)	2.79 (10)	1.28 (7)	1.15 (6)	0.97 (5)
Ce	28.5 (4)	42.3 (6)	8.2 (2)	3.20 (10)	2.18 (6)	1.86 (6)
Pr	3.72 (11)	6.75 (13)	1.49 (5)	0.53 (3)	0.46 (3)	0.38 (3)
Nd	17.7 (6)	37.0 (8)	8.6 (3)	2.9 (2)	2.6 (2)	2.3 (2)
Sm	4.0 (3)	9.0 (3)	3.2 (2)	1.23 (17)	0.99 (13)	0.85 (11)
Eu	1.50 (7)	3.10 (11)	1.30 (7)	2.18 (10)	0.68 (5)	0.57 (4)
Gd	4.8 (3)	12.3 (4)	4.5 (2)	2.9 (2)	1.52 (12)	1.29 (10)
Tb	0.69 (5)	1.95 (6)	0.73 (4)	0.52 (4)	0.30 (3)	0.26 (2)
Dy	5.3 (2)	14.0 (4)	5.5 (2)	4.1 (2)	2.36 (15)	2.03 (13)
Ho	1.09 (6)	2.93 (11)	1.19 (6)	0.99 (6)	0.46 (3)	0.39 (3)
Er	3.3 (2)	8.7 (3)	3.31 (13)	3.0 (2)	1.45 (10)	1.25 (8)
Tm	0.42 (3)	1.18 (5)	0.48 (3)	0.52 (3)	0.21 (2)	0.18 (2)
Yb	2.8 (2)	8.0 (2)	3.46 (16)	3.5 (2)	1.51 (9)	1.33 (8)
Lu	0.37 (4)	1.19 (5)	0.55 (3)	0.54 (4)	0.28 (2)	0.24 (2)
Hf	4.3 (2)	9.9 (3)	3.32 (14)	2.73 (14)	1.12 (9)	12.8 (3)
Ta	0.81 (4)	0.71 (2)	0.09 (1)	0.07 (1)	0.11 (1)	0.07 (1)
Tl	<0.15	<0.1	0.17 (3)	0.28 (6)	<0.1	0.04 (1)
Pb	10.0 (3)	2.70 (10)	1.60 (9)	1.13 (9)	14.9 (3)	12.8 (3)
Bi	0.29 (4)	0.07 (2)	<0.03	0.06 (2)	0.08 (2)	0.07 (1)
Th	0.75 (5)	0.92 (6)	0.10 (2)	0.18 (3)	0.04 (1)	0.04 (1)
U	0.38 (4)	0.61 (4)	0.10 (1)	0.16 (2)	<0.03	<0.03
Mg#	55.6	37.7	51.8	47.2	62.1	64.4
Eu*	1.05	0.90	1.06	3.54	1.69	1.66
La/Ta	15.1	22.5	29.9	18.3	10.7	10.7
La_N/Yb_N	3.12	1.44	0.58	0.26	0.54	0.52

FeO_{Tot}, total Fe; LOI, loss on ignition.
For major elements: nd, not detected.
For trace elements, uncertainties in last significant digit are indicated in parentheses.

Table 4 Whole-rock and trace element compositions of blueschists from the Bantimala Complex, South Sulawesi

Sample	BM03	BM04	BML01A	BML04A	BM05	BML03B	CP03C
Rock-type		Albite–epidote glaucophanite				Quartz glaucophane schist	
Whole-rock (wt%)							
SiO_2	50.84	40.69	46.76	45.17	57.77	59.27	63.75
TiO_2	0.82	4.55	2.72	1.29	0.98	1.08	1.01
Al_2O_3	14.17	13.07	13.16	15.97	13.81	13.65	12.46
FeO_{Tot}	10.55	19.32	11.80	11.04	9.52	9.68	8.19
MnO	0.20	0.66	0.17	0.17	0.22	0.40	0.17
MgO	8.73	10.48	9.03	4.70	5.29	4.82	4.64
CaO	6.59	2.90	7.81	10.68	3.77	2.54	4.71
Na_2O	3.14	2.39	2.95	3.65	3.12	2.94	2.30
K_2O	0.86	0.35	0.91	0.06	1.42	1.32	1.04
P_2O_5	0.10	0.03	0.67	0.08	0.15	0.10	0.10
SO_3	0.23	1.27	nd	nd	nd	0.05	0.55
F	nd	0.11	0.14	0.06	0.04	nd	0.02
Cl	nd	Nd	nd	nd	nd	nd	0.08
$-O \equiv F$	–	–0.05	–0.06	–0.03	–0.02	–	–0.01
$-O \equiv Cl$	–	–	–	–	–	–	–0.02
LOI	4.12	5.19	3.86	5.59	4.14	4.20	1.87
Total	100.34	100.97	99.92	98.44	100.20	100.05	100.85
Trace elements (µg/g)							
Be	0.54 (6)	0.57 (5)	2.10 (8)	0.48 (4)	0.98 (5)	1.22 (8)	1.04 (6)
Sc	34.5 (3)	49.6 (4)	29.9 (3)	40.5 (3)	29.3 (3)	31.8 (3)	30.0 (3)
V	354 (3)	644 (4)	269 (2)	353 (2)	219.4 (15)	219 (2)	213 (2)
Cr	394 (5)	23.8 (9)	50.1 (13)	28.3 (9)	248 (3)	298 (4)	311 (3)
Ni	162 (2)	86.4 (9)	115.0 (12)	21.7 (3)	92.3 (10)	128.5 (13)	93.8 (11)
Cu	97 (19)	2389 (20)	131.2 (12)	53.6 (7)	46.1 (13)	74.3 (9)	36.6 (5)
Zn	88 (3)	164 (2)	96.6 (11)	49.9 (8)	87.7 (10)	89.2 (10)	73.4 (14)
Ga	12.6 (2)	13.5 (2)	21.4 (3)	18.4 (3)	14.5 (2)	13.9 (2)	12.4 (2)
Ge	1.5 (2)	2.6 (2)	2.5 (2)	1.9 (2)	2.6 (2)	2.5 (3)	2.53 (11)
As	2.8 (7)	3.6 (2)	1.51 (10)	0.88 (14)	1.93 (16)	<0.4	1.21 (11)
Rb	16.5 (2)	8.03 (10)	18.7 (2)	0.85 (4)	33.0 (3)	33.3 (3)	28.1 (3)
Sr	166 (2)	44.5 (4)	432 (3)	895 (6)	230 (2)	107.7 (10)	208.5 (15)
Y	16.4 (2)	41.8 (4)	25.5 (3)	32.4 (3)	21.4 (2)	20.7 (2)	20.4 (2)
Zr	36.3 (5)	111.2 (12)	182 (2)	66.9 (6)	95.0 (9)	94.5 (10)	79.1 (8)
Nb	1.89 (5)	34.3 (3)	42.5 (4)	1.27 (4)	5.25 (9)	4.92 (10)	3.64 (8)
Mo	1.07 (7)	0.78 (5)	0.68 (5)	4.30 (15)	0.53 (4)	2.27 (12)	1.24 (11)
Ag	0.12 (2)	0.79 (4)	0.18 (2)	0.10 (2)	0.08 (2)	0.10 (2)	0.20 (2)
Cd	<0.1	<0.15	0.18 (6)	<0.1	<0.1	<0.15	<0.1
In	0.06 (1)	0.13 (1)	0.11 (1)	0.09 (1)	0.09 (1)	0.09 (1)	0.06 (1)
Sn	1.26 (11)	4.08 (11)	1.86 (9)	0.82 (7)	1.37 (8)	0.93 (8)	0.90 (7)
Sb	2.86 (11)	2.99 (10)	3.03 (11)	2.54 (13)	3.10 (9)	2.66 (11)	3.23 (9)
Cs	0.89 (3)	0.34 (2)	0.98 (3)	0.05 (1)	1.19 (3)	1.08 (4)	1.33 (5)
Ba	105 (2)	41.5 (4)	132.4 (11)	7.45 (13)	161.4 (14)	126.0 (12)	85.9 (8)
La	4.46 (10)	8.32 (13)	29.3 (3)	3.57 (8)	10.11 (14)	9.33 (14)	8.14 (11)
Ce	10.9 (2)	19.8 (2)	58.8 (7)	10.3 (2)	23.8 (3)	24.0 (3)	18.9 (2)
Pr	1.63 (5)	3.24 (7)	7.05 (11)	1.68 (5)	3.00 (6)	2.83 (7)	2.38 (6)
Nd	9.0 (2)	16.6 (4)	33.1 (6)	9.5 (2)	13.1 (3)	12.4 (3)	10.9 (3)
Sm	2.29 (16)	5.1 (2)	7.6 (2)	3.5 (2)	3.5 (2)	3.3 (2)	2.62 (14)
Eu	1.05 (6)	2.38 (8)	2.59 (8)	1.47 (6)	0.97 (4)	0.84 (4)	0.91 (4)
Gd	3.6 (2)	6.6 (2)	7.2 (2)	4.8 (2)	3.44 (13)	3.55 (13)	3.54 (14)
Tb	0.54 (3)	1.14 (3)	0.97 (3)	0.92 (3)	0.60 (3)	0.62 (3)	0.50 (2)
Dy	3.38 (15)	8.9 (2)	5.8 (2)	6.2 (2)	3.68 (14)	4.12 (16)	3.86 (15)
Ho	0.69 (3)	1.72 (4)	0.96 (4)	1.27 (5)	0.84 (4)	0.83 (4)	0.76 (3)
Er	1.92 (9)	5.11 (13)	2.26 (12)	3.46 (13)	2.53 (10)	2.37 (12)	2.35 (10)
Tm	0.23 (2)	0.77 (2)	0.28 (2)	0.49 (2)	0.37 (2)	0.38 (3)	0.36 (2)
Yb	1.73 (10)	5.09 (15)	1.59 (7)	3.33 (11)	2.49 (11)	2.29 (9)	2.24 (9)
Lu	0.28 (2)	0.77 (3)	0.23 (2)	0.53 (3)	0.36 (2)	0.42 (3)	0.30 (2)
Hf	1.49 (7)	3.23 (11)	5.26 (14)	2.77 (11)	3.65 (12)	4.57 (16)	3.80 (12)
Ta	0.13 (1)	0.94 (2)	1.02 (2)	0.20 (1)	0.20 (1)	0.22 (1)	0.13 (1)
Tl	0.16 (3)	0.06 (2)	0.13 (3)	<0.05	0.19 (4)	0.25 (5)	0.17 (3)
Pb	2.6 (8)	0.71 (8)	7.2 (2)	17.2 (3)	5.9 (2)	2.93 (15)	5.37 (13)
Bi	0.05 (2)	0.18 (2)	0.06 (1)	0.08 (2)	0.09 (2)	0.05 (2)	0.10 (1)
Th	0.44 (4)	0.33 (3)	3.46 (9)	0.20 (2)	1.81 (6)	1.72 (7)	1.20 (4)
U	0.18 (2)	0.15 (2)	0.99 (5)	0.10 (1)	0.61 (3)	0.54 (4)	0.52 (3)
Mg#	45.3	35.2	43.4	29.9	35.7	33.2	36.2
Eu*	1.05	1.20	1.04	1.09	0.83	0.73	0.91
La/Ta	33.3	8.8	28.6	17.6	51.0	41.8	62.6
La_N/Yb_N	2.3	1.4	16.1	0.95	3.5	3.5	2.6

sFeO$_{Tot}$, total Fe; LOI, loss on ignition.
For major elements: nd, not detected.
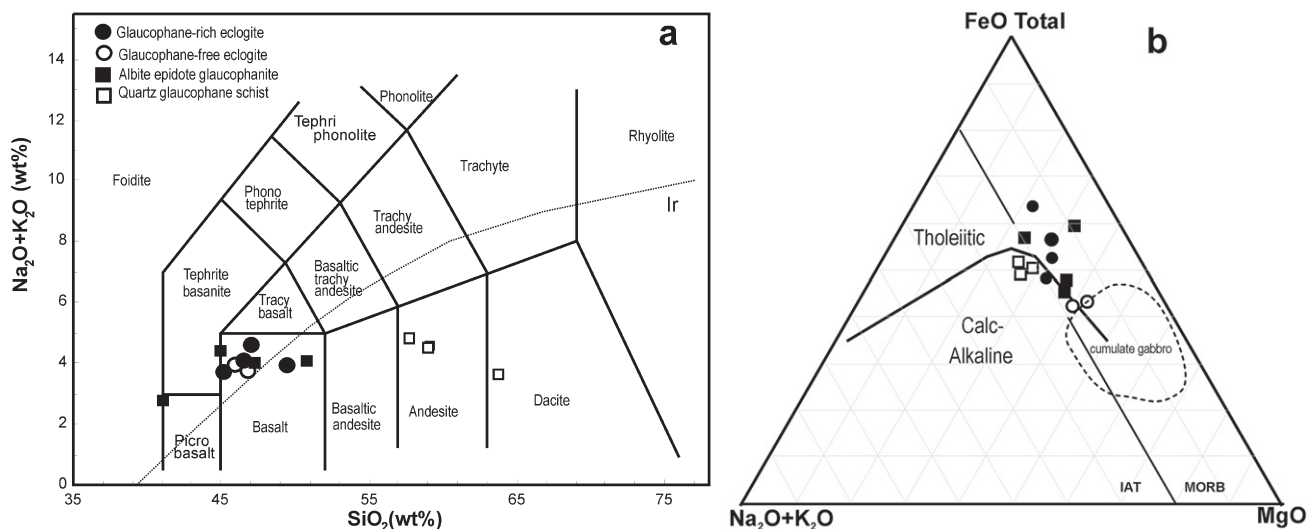For trace elements, uncertainties in last significant digit are indicated in parentheses.

Fig. 4   (a) TAS diagram (Le Bas *et al*. 1986) for eclogites and blueschists from Bantimala Complex, South Sulawesi. SiO_2 and Total Alkali are in wt%. The dividing line 'Ir' separates alkaline from subalkaline rocks, after Irvine and Baragar (1971). (b) Eclogite and blueschist compositions plotted in the FeO_{Total}-Alkali-MgO ternary diagram of Irvine and Baragar (1971). Dashed region indicates cumulate gabbros from the Southwest Indian Ridge (Meyer *et al*. 1989) and the Mid-Atlantic Ridge (Tiezzi & Scott 1980) are plotted for comparison.

andesite and dacite fields. Hence, the current positions of the rocks in the TAS diagram still correspond to those of subalkaline ultramafic–intermediate rocks, even though their current compositions may deviate from those of their protoliths. The diagram shows no evidence that the samples lie on a single evolutionary trend. The enrichment of Fe in the albite–epidote–glaucophanites reveals their tholeiitic nature in an AFM (Alkalis–FeO_{Total}–MgO) diagram (Fig. 4b). The quartz–glaucophane schists have a high SiO_2 content which places them on the edge of the calc-alkaline field. However, the Cr content of these rocks (248–311 µg/g: Table 4) is towards the high end of the range exhibited by the other rock types (Tables 3,4). It is possible that the quartz–glaucophane schists are derived from mafic protoliths, but have been altered by SiO_2-rich fluids. Another possibility is that they represent tectonic mixtures of a mafic composition with a silicic, alkali-rich material that is nevertheless high in Cr, such as greywacke containing detrital Cr-rich spinel. Typical greywacke compositions such as the averages tabulated by Condie (1993) have $SiO_2 = 65$–66 wt% and about 5 wt% ($Na_2O + K_2O$), placing them at the alkaline end of the 'dacite' field in Figure 4a and squarely in the 'calc-alkaline' field of Figure 4b. However, some aspects of the composition favour the metasomatic alternative, as discussed below.

The Al_2O_3–TiO_2 discrimination plot of Spandler *et al*. (2004) separates the eclogites into distinct populations on the basis of TiO_2 contents, as seen in Figure 5. The glaucophane-rich eclogites plot in the relatively high-Ti MORB field except for very high-Ti BM15B and low-Ti CP03E, the latter of which plots with the glaucophane-free eclogites in the cumulate gabbro field. The albite–epidote glaucophanites were similarly varied. Samples BM04 and BML04 plotted in the MORB basalt field, whereas BML01 plotted in the oceanic island basalt (OIB) field and BM03 lay in the cumulate field, along with the quartz–glaucophane schists. However, we note that the Al_2O_3 and TiO_2 contents of the quartz–glaucophane schists may have been reduced by contamination or alteration, so the original slightly higher values may have placed them in the MORB field.

As expected, correlation between chemical composition (Tables 3,4) and mineral mode (Table 1) exists not just for major elements, but also for trace elements that are concentrated into specific host minerals. Ba contents show a positive correlation with modal abundance of phengite in most samples except for sample BML04, which is very low in Ba and other large ion lithophile (LIL) elements, and Sr contents of all samples show a good relationship with epidote abundance. Since zircon is either 'present' or 'absent', we cannot correlate Zr content and zircon except very crudely: the four highest-Zr samples are indeed the four samples with abundant zircon. However, Ti contents do not correlate with estimated modes of rutile or titanite. This is probably due to heterogeneous or
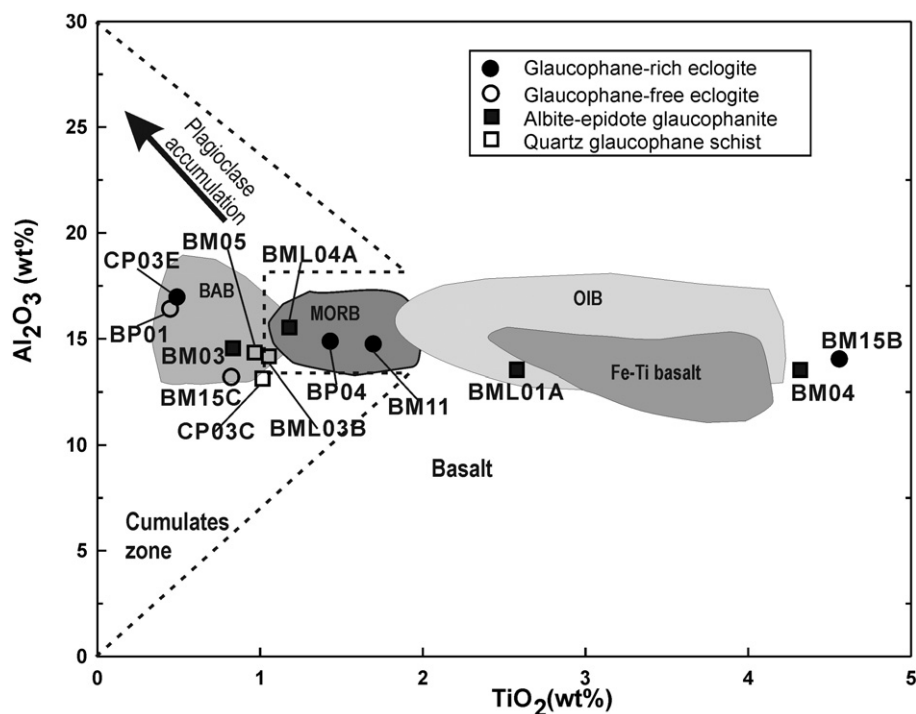
Fig. 5 Al$_2$O$_3$ *vs* TiO$_2$ diagram after Spandler *et al.* (2004), showing bulk-rock compositions for the Bantimala Complex eclogite- and blueschist-facies rocks. Al$_2$O$_3$ and TiO$_2$ are in wt%. BAB, BacK–Arc Basin; MORB, Mid-Ocean Ridge Basalt; OIB, Oceanic Island Basalt. Data for the field of various basalt types are from Saunders and Tarney (1984), Sinton and Fryer (1987), Sun and McDonough (1989) and Wilson (1989).

clumped distribution of Ti minerals in the sample. Apatite modes are too low for a reliable correlation with P content.

In order to identify the post-magmatic element mobility during high-pressure metamorphism, selected major and trace elements are plotted against Zr diagrams (Fig. 6), since Zr is moderately incompatible and shows restricted mobility in a variety of post-magmatic processes (Cann 1970; Pearce & Norry 1979; Sheraton 1984; Kullerud *et al.* 1990).

Out of the diagrams of Figure 6, Zr *vs* Ti, Y, and Nb show strong positive correlations with only one or two outlying points, suggesting that these elements have not been mobile during metamorphism. A positive correlation is also visible for Fe, albeit with more scatter. Relatively flat trends with some scatter for Na, Al, and Si suggest that the same is broadly true for these elements, although the quartz–glaucophane schists are clear outliers in the Si plot, due to their elevated SiO$_2$ content. Conversely, broad scatter is seen for K, Ca, Cr, Ni, Rb, and Sr. For the large ion lithophiles K, Ca, Rb, and Sr, this presumably correlates with mobility of these elements during high-pressure metamorphism. The plot for Ba (not shown) is very similar to that for K (cf. Figure 10 below). Note that the quartz–glaucophane schists are very high in K and Rb, but are low in Na, Ca, and Sr, which suggests that the source of the excess SiO$_2$ was more

likely metasomatism by a fluid than mixture with plagioclase-rich sediment. The variations in less mobile but highly compatible transition metals such as Cr and Ni presumably reflect the original protolith mineral chemistry. The unusually high P$_2$O$_5$ content in sample BML01A presumably reflects high modal apatite; the phosphorus may be derived from admixed sediments.

TRACE ELEMENT SYSTEMATICS

All the glaucophane-rich eclogites are enriched in mobile large ion lithophile elements (LILEs) such as Rb and Ba (20–50 × Primitive Mantle except BM15B with lower abundances). Similarly, all show a positive Sr anomaly except for BM15B, which has a negative anomaly (Fig. 7a). All except CP03E show a positive Ti anomaly. Concentrations of high field-strength elements (HFSE) such as Nb, Ta, Zr, Hf in BP04 and CP03E are similar to those of glaucophane-free eclogite, but are an order of magnitude higher in the case of BM11 and BM15B. Nb and Ta for BP04 and CP03E are depleted relative to their neighbouring elements in the spidergram, which is not true for the glaucophane-free eclogites. Chondrite-normalized rare earth element (REE) patterns for the glaucophane-rich eclogites show three distinct types (Fig. 7b). The first group (BM11 and BM15B) shows enrichment in light rare earth
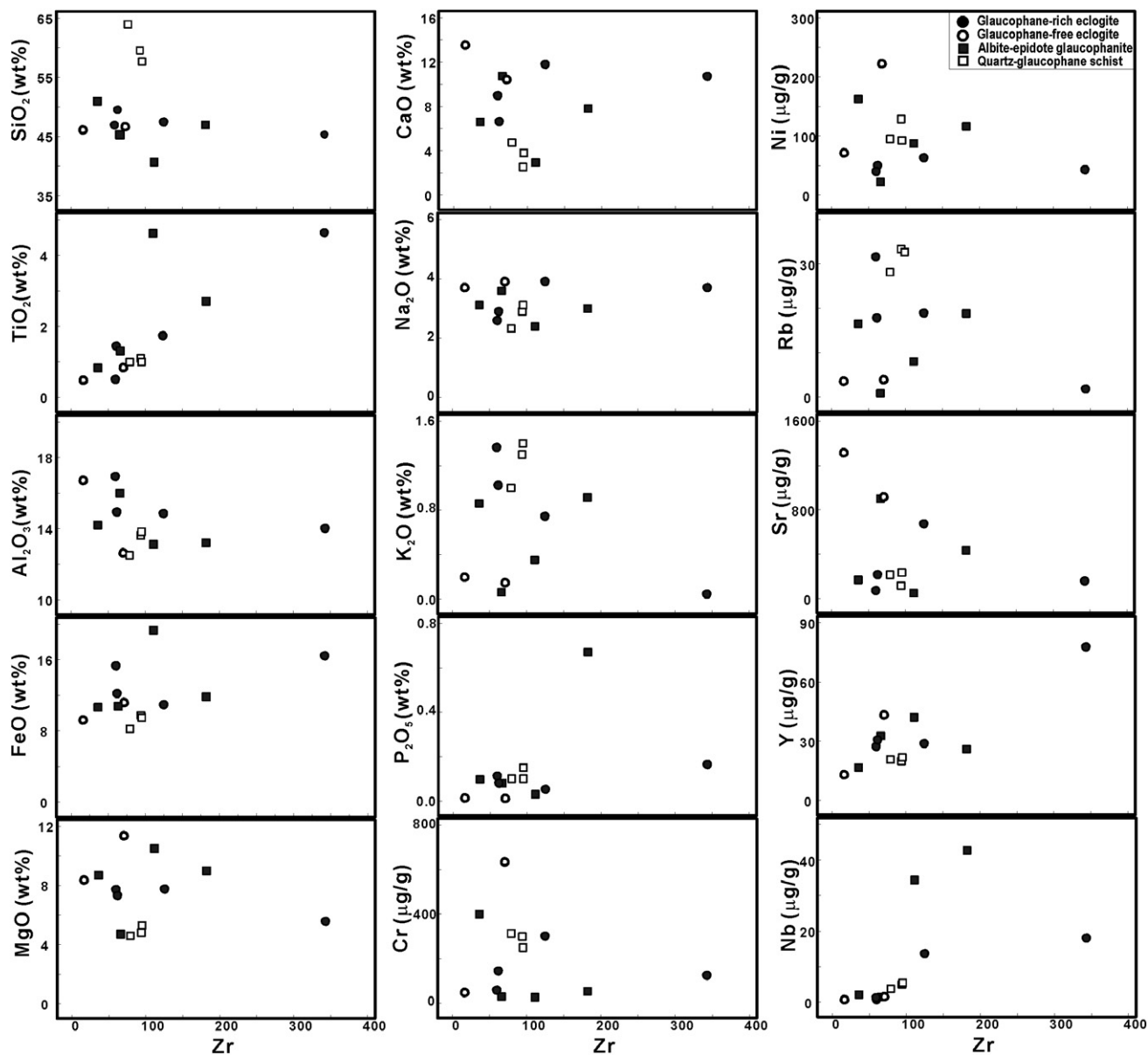
Fig. 6   Element *vs* Zr plots for the eclogite- and blueschist-facies rocks from the Bantimala Complex. 'FeO' is total Fe, expressed as FeO.

element (LREE) (La$_N$/Yb$_N$ = 1.4–3.1) without noticeable Eu anomalies (Eu/Eu* = 0.9–1.0), and flat heavy rare earth elements (HREE). The second type consists solely of BP04, with relatively depleted LREE (La$_N$/Yb$_N$ = 0.3) and almost flat HREE. The last type is represented by CP03E, showing depletion in LREEs (La$_N$/Yb$_N$ = 0.6), positive Eu anomaly (Eu/Eu* = 3.6), and nearly flat HREE. The positive Eu anomaly further suggests that the protolith accumulated plagioclase in the magma chamber.

The glaucophane-free eclogites have moderate enrichment of the mobile LILE, Rb and Ba (5–15 × PM), but a very large positive Sr anomaly

in the primitive mantle-normalized trace element diagrams (Fig. 7c). The Sr anomaly in the eclogites may originally have been due to seawater alteration, subsequently preserved by abundant epidote in the high-pressure mineral assemblage, which is a highly compatible host for Sr. The high modal proportion of clinopyroxene in eclogite may also have contributed to retention of high Sr (Sassi *et al.* 2004). The Sr anomaly may have been further enhanced by plagioclase accumulation, as evident from the REE data. Chondrite-normalized REE patterns show LREE depletion (La$_N$/Yb$_N$ = 0.54–0.52) similar to N-MORB, but systematically depleted in concentration by a factor of
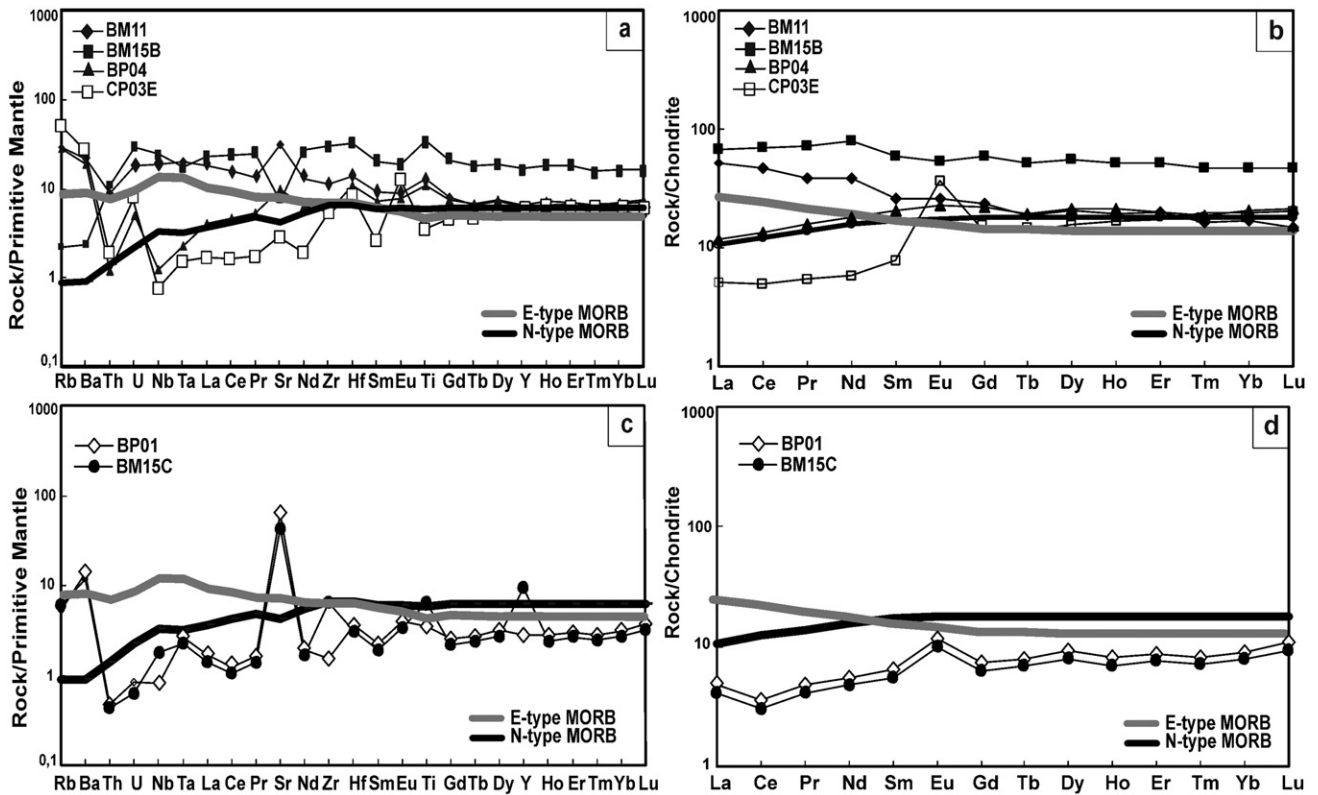
Fig. 7 Trace and rare earth element patterns of glaucophane-rich (a, b) and glaucophane-free (c, d) eclogite from the Bantimala Complex. Normalization values are from Sun and McDonough (1989).

2–3 (Fig. 7d). There is a distinctive positive Eu anomaly (Eu/Eu* = 1.6–1.7). Both the Sr and Eu anomalies suggest accumulation of plagioclase during the formation of these rocks. A very small negative Ce anomaly may imply slight alteration (Ludden & Thompson 1979; Desprairies & Bonnot-Courtois 1980) or contamination by continental crust (Defant *et al.* 1991).

The primitive mantle-normalized trace element patterns of the albite–epidote–glaucophanites show a wide range of affinities. They can be classified into three types. The first type (BM04 and BML04A) is less enriched in the more mobile LILE and relatively enriched in HFSE (Fig. 8a). However, BM04 is not as depleted in Ba and Sr as BML04A. Chondrite-normalized REE of BML04A show slight LREE enrichment ($La_N/Yb_N = 0.95$), no Eu anomaly and flat HREE (Fig. 8b), whereas sample BM04 has more LREE enrichment ($La_N/Yb_N = 1.2$). The patterns bear some resemblance to E-MORB for BM04 and N-MORB for BML04A, but with considerable perturbations. The second type (BML01A) is characterized by greater enrichment of LILE and HFSE than N-MORB or E-MORB patterns,

but closely follows the oceanic island basalt trend (Fig. 8c). Consistent with this, chondrite-normalized REE (Fig. 8d) show strong LREE enrichment ($La_N/Yb_N = 16$) and an overall negative slope for REE, without significant anomaly of Eu. The last type (sample BM03) is distinguished by strong enrichment of LILE and depletion in Nb and Ta (Fig. 8e), indicating an island arc affinity. Chondrite-normalized REE show enrichment of LREE ($La_N/Yb_N = 2.3$) without significant Eu anomaly (Eu/Eu* = 1.05) (Fig. 8f).

Primitive mantle-normalized trace elements from the quartz–glaucophane schists show relatively uniform patterns, which are all very similar to those of BM03 and show the same depletion in Nb and Ta (Fig. 8e,f). They show enrichment of LILE (Rb, Ba, Th, and U) relative to HFSE (Fig. 8e). Chondrite-normalized trace elements show enrichment in LREE ($La_N/Yb_N = 2.6–3.5$) with slight negative Eu anomalies (Eu/Eu* = 0.7–0.9) and relatively flat HREE (Fig. 8f). Enrichment in large ion lithophiles is consistent with the depletion in HFSE being originated in an island arc setting, but has probably been enhanced due to alteration during subduction (cf. Fig. 6).
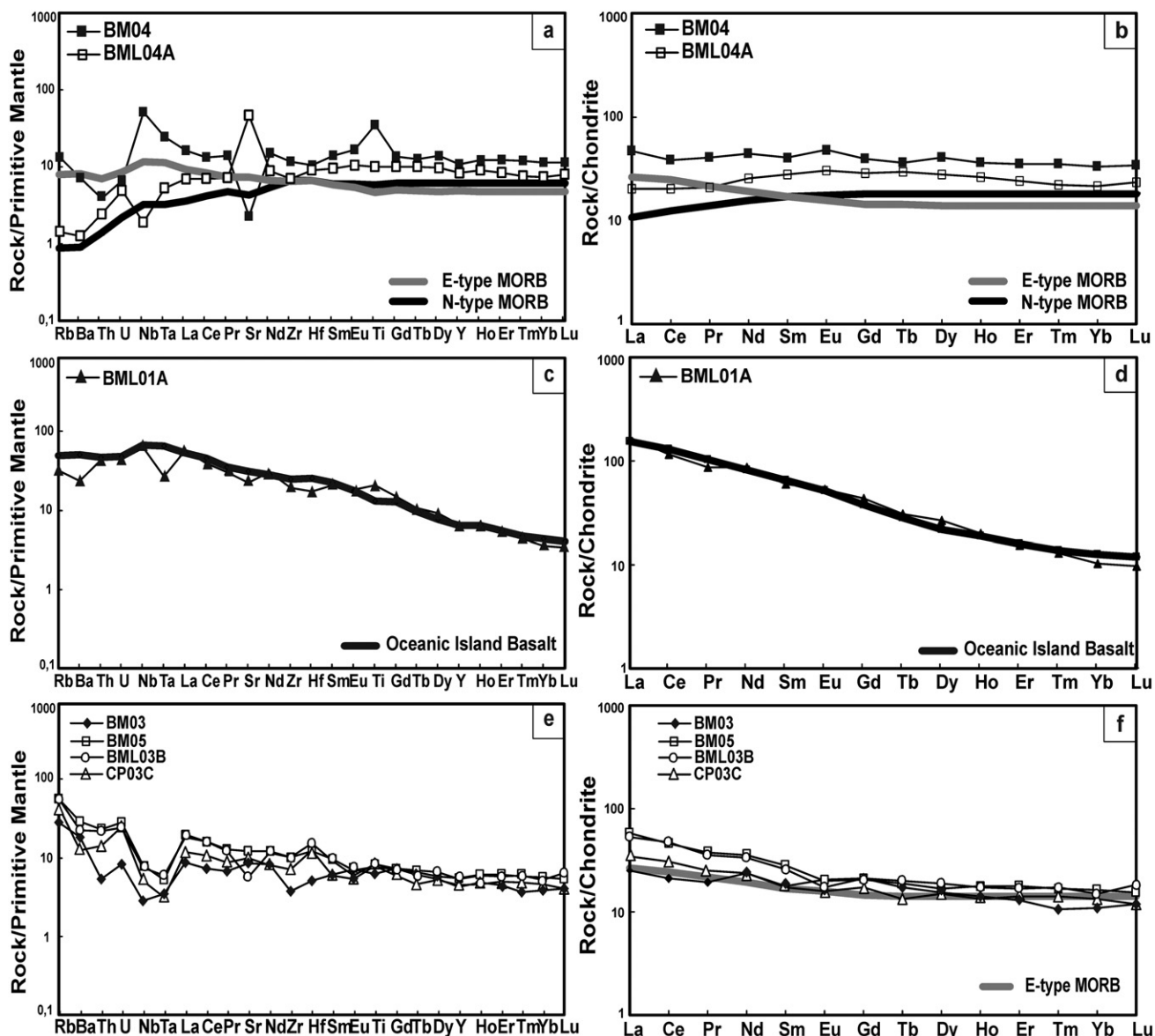
Fig. 8 Trace and rare earth element patterns of albite–epidote glaucophanite. Normalization values are the same as in Figure 7. (a,b) BM04 is E-MORB-like, while BML04A resembles N-MORB. However, anomalies indicate that they are actually of oceanic Island and island arc basalt type, respectively. (c,d) BML01A resembles typical oceanic island basalt. (e, f) BM03, BM05, BML03B and CP03C show typical subduction affinities with Nb and Ta depletion. Data for the field of N-MORB, E-MORB and OIB are from Sun and McDonough (1989).

DISCUSSION

The major and trace element geochemistry can potentially reveal much about the original protolith and the tectonic setting in which it originated, as well as processes which have affected it subsequently. However, in interpreting the geochemical data, we need to be aware of potential biases and limitations in the data. The main issues are:

(i) To what degree is the the hand sample is representative of the larger-scale outcrop?

(ii) How far have the elemental contents of the rock been changed from their pristine igneous values as a result of alteration on the seafloor and during subduction?

Logistical constraints on sample size may have resulted in some minerals being over- or under-represented in the sample. Sampling error is most likely to occur for elements that are concentrated in rare accessories such as zircon, or in large porphyroblasts such as garnet in eclogite. Unrepresentative modes of such minerals show up as anomalous major and trace element concentrations enriched in those minerals. In the examples given, Zr, Hf and probably U would correlate strongly with zircon content, and heavy REE with

garnet. Fortunately, our datasets show no egregious examples of such anomalies in mode and trace element content.

There is evidence that HFSE such as Ti, Zr, Nb Y, and REE are effectively insoluble and immobile during subduction and metamorphism (Thompson 1973; Sheraton 1984; McCulloch & Gamble 1991; Pearce *et al.* 2000; Zhao *et al.* 2007). Hence, these elements conserve their original contents and ratios, and provide insight into the paleo-environment of the subducted rocks (Pearce & Norry 1979; White 2007). Conversely, the relatively mobile LIL elements, such as Rb and Ba, are very incompatible in mafic rocks and hence are more likely to be mobile and undergo change during metamorphism. Thus, these elements are useful petrogenetic indicators of modification rather than of the original protolith (Sorensen *et al.* 1997). Plots of LIL *vs* HFSE content such as those in Figure 6 can be used to check for such modification. Contamination by fluids or sediments is indeed evidenced in our quartz–glaucophane schists, which show elemental concentrations that are inconsistent with a pristine igneous protolith: these are nevertheless included in the discussion below, with appropriate caveats.

NATURE OF THE PROTOLITHS

On the basis of major elements (particularly TiO_2 content), the glaucophane-rich eclogites all plot in the MORB field except for CP03E, whereas the glaucophane-free eclogites lie in the cumulate field (Fig. 5). This feature is consistent with the trace element and REE data.

Based on primitive-mantle normalized trace elements and chondrite-normalized REE patterns, glaucophane-rich eclogites BM11 and BM15B correspond to evolved (fractionated) E-MORB, in which the removal of olivine has increased the concentration of REE. Conversely, BP04 resembles N-MORB, whereas CP03E is a plagioclase-rich cumulate. The data, when plotted on the Hf–Ta–Th diagram of Wood (1980) support the idea that these eclogites are derived from more than one type of MORB (Fig. 9a). The absence of positive Eu anomaly from this group (except sample CP03E) further supports their origin as basalts rather than cumulates. La/Ta ratios between 15 and 22 are within the MORB range (average 18.5; Saunders 1984). The more evolved composition of the source for sample BM15B is also supported by enrichment of less compatible elements (TiO_2 and Y) and depletion of more compatible (MgO, Cr, and Ni) elements, as shown in the diagrams of Figure 6.

Incompatible trace element contents of the glaucophane-free eclogites (Table 3) are relatively lower than for the glaucophane-rich eclogites, suggesting that the protolith is cumulate gabbro rather than basalt. The chondrite-normalized REE abundance of the glaucophane-free eclogites is more depleted than N-MORB and has a positive Eu anomaly, which can be attributed to enhanced Eu by plagioclase accumulation. Cumulate gabbros can be distinguished from basalts by their lower TiO_2 and higher Mg# and Pb. Furthermore, the glaucophane-free eclogites also plot in or near the cumulate gabbro field in an AFM diagram (Fig. 4b). Therefore, the glaucophane-free eclogites are interpreted to be derived from cumulate gabbros which formed in a mid-oceanic ridge setting. They show a similar REE pattern to metagabbro from the Pohorje eclogite (Sassi *et al.* 2004) and type V eclogite from New Caledonia (Spandler 2004). However, no textural information remains to confirm the gabbroic origin. All the eclogites lie in the 'N-MORB' or 'E-MORB' field on the Th–Hf–Ta diagram of Wood (1980), implying that they formed in an extensional setting with minimal crustal contamination (Fig. 9a).

We deduce a range of protoliths for the blueschists, consistent with their wide variation in trace and rare earth elements. The primitive mantle-normalized pattern of BML04A, in general, shows a typical downward-curving N-MORB pattern, whereas the enrichment of LREE and HFSE in BM04 gives it an upward curve with an E-MORB affinity (Fig. 8a). Samples BML04A and BM04 also plot in the fields of N-MORB and E-MORB, respectively, in the Hf–Ta–Th diagram of Wood (1980) (Fig. 9a) and BML04A in the N-MORB fields of the Nb–Zr–Y diagram of Meschede (1986) (Fig. 9b) and the Zr–Ti–Y diagram of Pearce and Cann (1973) (Fig. 9c). However, sample BML04A also shows a positive anomaly in Sr and negative anomalies in Nb and possibly Ta, which suggests that it is actually from an island arc régime. Conversely, BM04 plots in the 'within-plate alkaline' field of Figure 9b, and outside any fields in Figure 9c, although it is close to the 'within-plate' field. This is because it shows strong enrichment in Ti, Nb and Ta, consistent with oceanic island origin.

A more obviously non-MORB sample, BML01A, is characterized by the greater enrichment of LILE and HFSE than the N-MORB pattern, combined with the negative slope for Sm – Yb, typical
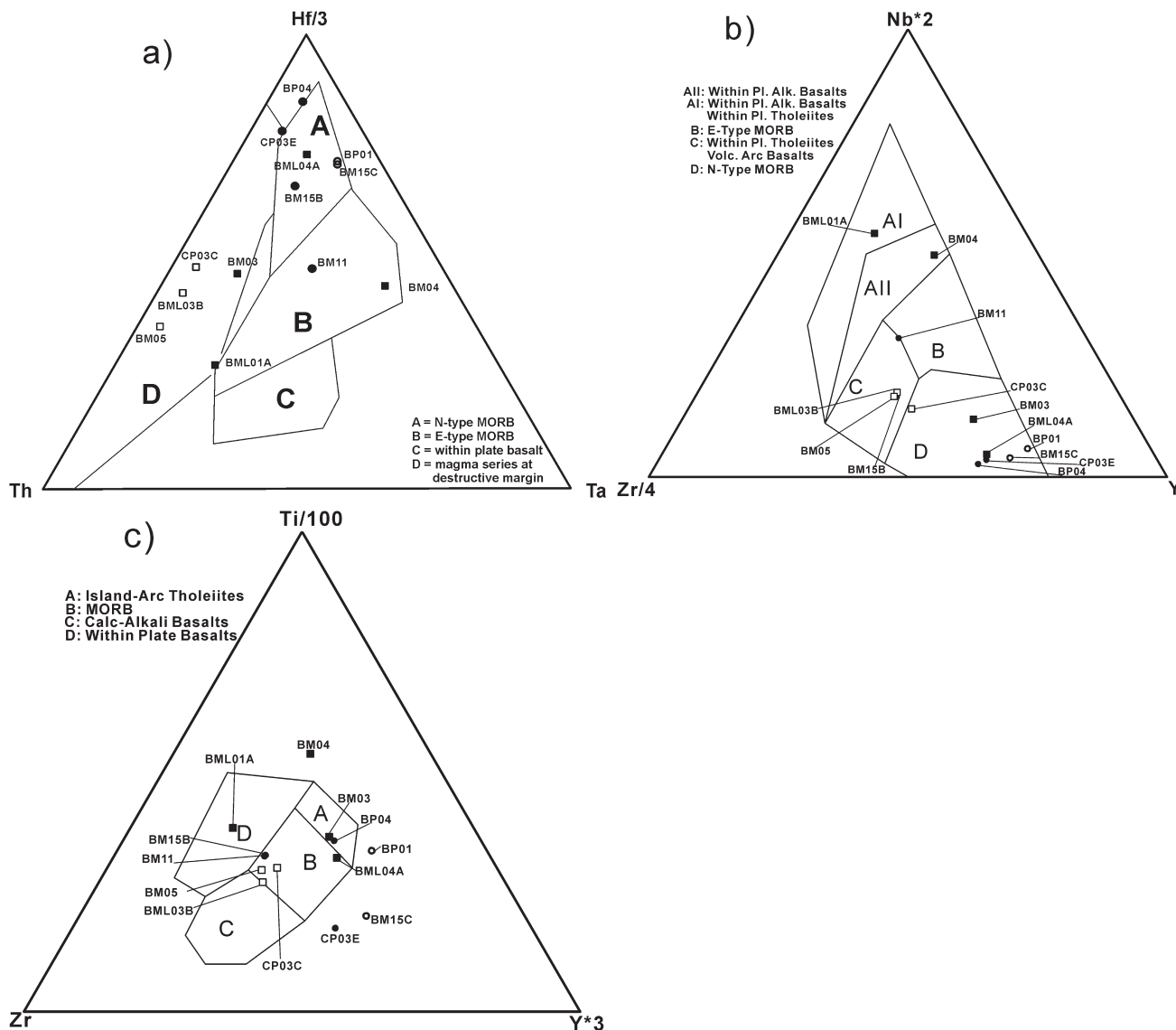
Fig. 9 (a) Th-Ta-Hf discrimination diagram for basalt (Wood 1980) showing Bantimala eclogites and blueschists. (b) Nb – Zr – Y discrimination diagram (Meschede 1986) (c) Ti – Zr – Y discrimination diagram (Pearce & Cann 1973).

of oceanic island tholeiitic basalt (Holm 1985). Chondrite-normalized REEs of this sample show strong LREE enrichment without significant Eu anomalies, and resemble the oceanic island pattern of Sun and McDonough (1989) and the pattern of enriched seamount samples in the eastern Pacific (Niu & Batiza 1997). The trace element contents of this sample also show a good agreement with the group III eclogite from Zambia of John *et al.* (2004), which is derived from oceanic island basalt. Furthermore, the sample plots in the within-plate basalt field in the Nb–Zr–Y and Ti–Zr–Y diagrams (Fig. 9b,c).

BM03 appears to have originated as an IAB as shown by the typical arc signatures in its trace-

element spidergram (depletion of Nb and Ta; Fig. 8e). The La/Ta ratio of this sample is typical for arc basalt (>30; e.g. Perfit *et al.* 1980). The low TiO₂ concentration and relative LREE enrichment of sample BM03 are characteristic of island arc volcanic rocks (Perfit *et al.* 1980; Sorensen *et al.* 1997). In addition, this sample plotted in the destructive margin field in the diagram of Wood (1980) and in the island arc tholeiitic field in the-diagram of Pearce and Cann (1973), as shown in Figure 9a and c.

A summary of the protoliths deduced for the Bantimala Complex eclogites and blue-schists is given in Table 5. Note that the various discriminants employed in Figures 6–9 do not all
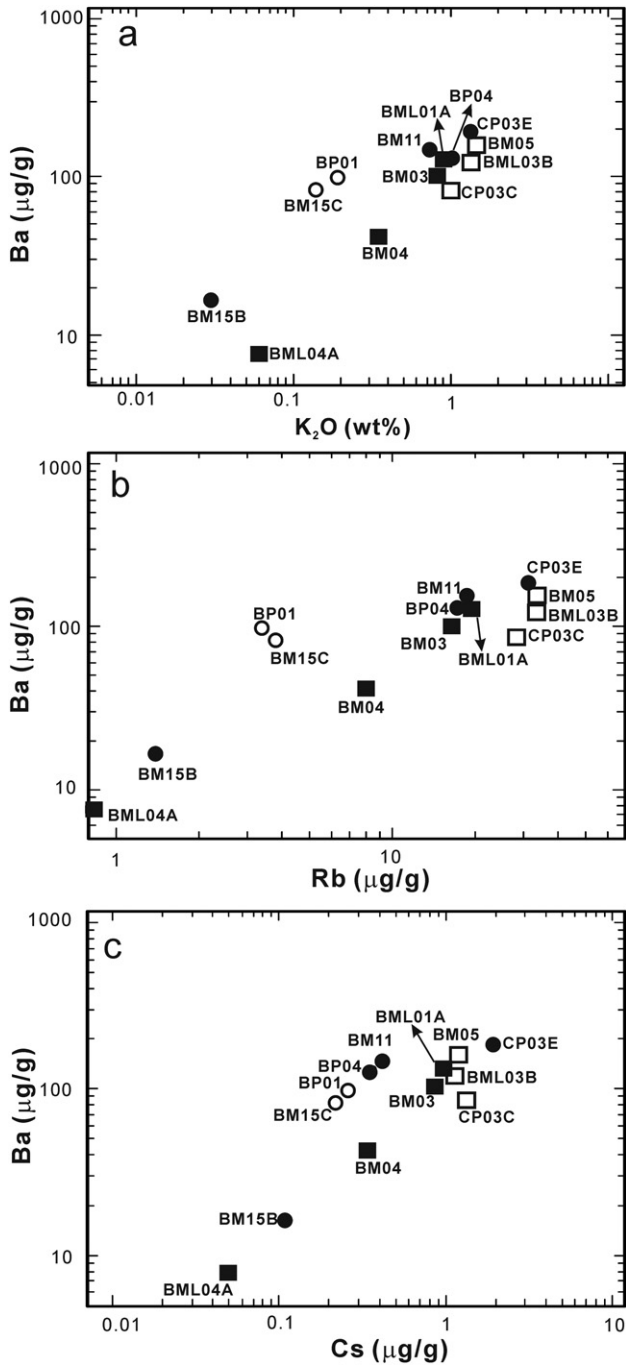
Fig. 10 Barium content *vs* (a) K, (b) Rb and (c) Cs for the studied samples. Symbols are as in Figure 4.

distinguish the same sets of mafic rock types, and are not always in perfect agreement on how they classify a given sample. However, a consensus on classification is always apparent.

SYSTEMATICS OF K, Rb, Ba, and Cs

Sorensen *et al.* (1997) reported an enrichment of LILE, particularly K, Rb, Ba, and Cs during

Table 5 Protoliths for mafic rocks of the Bantimala Complex, as indicated by various discrimination methods, and overall consensus.

Sample	Current Lithology	TiO$_2$-Al$_2$O$_3$ (Fig. 5)	Spidergrams (Figs 7, 8)	Th-Hf-Ta (Fig. 9a)	Zr-Nb-Y (Fig. 9b)	Zr-Ti-Y (Fig. 9c)	Consensus Protolith
BM03	Ab-Ep Glaucophanite	Cumulate/BAB	IAB	IAB	N-MORB	IAB	IAB
BM04	Ab-Ep Glaucophanite with eclogite relicts	[very high Ti]	OIB	E-MORB	OIB	OIB?	OIB
BM05	Qtz-Gln Schist	Cumulate/MORB	IAB	IAB	OIB/IAB	MORB	IAB
BM11	Gln-rich Eclogite	MORB	E-MORB	E-MORB	OIB/IAB/E-MORB	MORB	E-MORB
BM15B	Gln-rich Eclogite	[very high Ti]	E-MORB	N-MORB	OIB/IAB	MORB	Cumulate
BM15C	Gln-free Eclogite	Cumulate/BAB	Cumulate	N-MORB	N-MORB		Cumulate
BML01A	Ab-Ep Glaucophanite	OIB	OIB	IAB/E-MORB	OIB	OIB	OIB
BML03B	Qtz-Gln Schist	Cumulate/MORB	IAB	IAB	OIB/IAB	MORB/Calc-alkaline	IAB
BML04A	Ab-Ep Glaucophanite	MORB	IAB	N-MORB	N-MORB	MORB	IAB
BP01	Gln-free Eclogite	Cumulate/BAB	Cumulate	N-MORB	N-MORB		Cumulate
BP04	Gln-rich Eclogite	MORB	N-MORB	N-MORB	N-MORB	IAB	N-MORB
CP03C	Qtz-Gln Schist	Cumulate/MORB	IAB	IAB	OIB/IAB/N-MORB	MORB	IAB
CP03E	Gln-rich Eclogite	Cumulate/BAB	Cumulate	N-MORB	N-MORB		Cumulate

BAB, back-arc basin basalt; Cumulate, gabbroic cumulate; IAB, island arc basalt ('destructive plate margin' setting of Fig. 9); OIB, oceanic island basalt ('within-plate' setting of Fig. 9).

high-pressure metamorphism in eclogite and related rocks from the Franciscan Complex. Enrichment of LILE during high-pressure metamorphism is also reported by Zack *et al.* (2001), John *et al.* (2004) and Bebout *et al.* (2007). Most of the eclogite- and blueschist-facies samples from the Bantimala Complex show enrichment of these elements, except BM15B (Fig. 10a–c). It can be seen that K, Ba, Rb, and Cs are strongly correlated, and that the correlation is similar in blueschist- and eclogite-facies samples, suggesting that LILE enrichment was controlled by the same process throughout. Phengite is the main host for LILE in high-pressure metamorphic rocks (Sorensen *et al.* 1997; Zack *et al.* 2001; Bebout *et al.* 2007). Note that the LILE are relatively higher in glaucophane-rich eclogite sample CP03E, consistent with the higher modal composition of phengite in this sample (Table 1).

TECTONIC SETTING

The geochemical analyses show that the protoliths of the eclogites and blueschists were all of tholeiitic affinity, but formed in a variety of different tectonic settings (Table 5). One (BML01A), now a blueschist, is strongly indicated to have been an OIB, and another shows more subtle OIB characteristics. Five appear to have derived from island arc basalt formed at a convergent plate boundary. Two derived from normal and enriched MORB originated in an extensional setting. The remaining four samples are gabbroic cumulates, geochemically similar to MORB, suggesting that they, too, formed at ridges. The Bantimala subduction zone evidently consumed geochemically varied portions of ridge-generated crust, along with seamounts (OIB) and a volcanic arc. The cumulates and most of the MORB protolith were subducted deep, to eclogite-facies P/T conditions, while the others, perhaps due to their occurrence in thicker crust, were subducted only to blueschist-facies P/T conditions. The degree of deformation during metamorphism was variable, irrespective of subduction depth. While some samples are strongly recrystallized and foliated, others retain relicts of the original igneous structure, such as a pillow structure in glaucophane-rich eclogites (Fig. 2a,b). Each of the tectonic settings was represented in two or three of the river sections of this study, implying that small tectonic slices have been intimately mixed in this accretionary complex.

Previous models of plate tectonics for the South Sulawesi region, particularly the Bantimala Complex, have been formulated using geological and seismic as well as geochronological data (Wakita *et al.* 1996; Guntoro 1999). The Bantimala Complex is generally considered as a result of subduction of oceanic crust under continental West Kalimantan, followed by exhumation of high-pressure metamorphic rocks. However, the protoliths of the high-pressure metamorphic rocks were not well-constrained. This study is the first to report bulk-rock geochemical data for high-pressure rocks from the Bantimala Complex. This data allows us to identify the protolith types that were subducted, the tectonic settings in which they formed, and hence provides a picture of the ocean floor that was subducted.

The ocean that lay to the east of the Bantimala Complex subduction zone is known to have been complex in paleogeography. Continental fragments are preserved just to the east, which are probably of Australian (Gondwana) origin, moving in on the subducting oceanic plate from the east in the late Jurassic. Collisions involving such fragments have been described by previous workers (e.g. Audley-Charles *et al.* 1972; Audley-Charles 1983; Metcalfe 1998). Evidence of such continental fragments in the Bantimala area is represented by the Jurassic shallow-marine sedimentary rocks (the Paremba Sandstone) which consist of conglomerate, sandstone and shale. In addition, the sample BM03 shows an island arc character. The quartz–glaucophane schists probably do so as well, although these samples have undergone significant SiO_2–LILE metasomatism. Hence, a portion of a volcanic arc was subducted in the Bantimala subduction zone. Seamounts also arrived in the subduction zone, along with oceanic crust including both N- and E-MORB types, mafic cumulates and deep-marine sediments. All units were then metamorphosed at high pressure in the subduction zone. Subsequently, slab fragments representing all these types were exhumed, from depths of >90 km for the eclogite-facies rocks, less for the blueschists, including the rocks derived from an arc and seamounts. A high peak metamorphic pressure is indicated by the high Si content of phengite (3.4 a.p.f.u.) in the eclogites. Miyazaki *et al.* (1996) calculated P/T conditions (580–630°C at 1.8 GPa to 590–640°C at 2.4 GPa), implying a low geothermal gradient (8°C/km) consistent with a high rate of subduction of a cold oceanic plate. Even higher peak pressures (>2.7 GPa) were implied by the later finding of coesite inclusions

within garnet and zircon (Parkinson & Katayama 1999). Maulana (2009) reported similar high pressures for the eclogite-facies rocks (up to 2.8 GPa at 550–620°C). Uplift must have been rapid, in order to avoid overprinting of the relatively low-temperature blueschists and eclogites. The rapid exhumation may have been driven by buoyancy after slab break-off, or may be related to the extension associated with rollback of the subducting slab, as suggested for exhumation in the New Caledonia high-P belt (Spandler 2004).

CONCLUSIONS

Whole-rock major and trace element compositions of the eclogite- and blueschist-facies rocks from the Bantimala Complex have been obtained. Geochemical criteria have been used to identify the protoliths as derived from various tectonic environments: island arc basalt, oceanic island basalt, mid-ocean ridge basalt, and cumulates. Chemical compositions indicate that the eclogites are derived from MORB and cumulate gabbro, whereas blueschists are mainly derived from oceanic island basalt and island arc basalt. The Bantimala Complex results from late Jurassic westward subduction near the Sundaland margin of oceanic seafloor bearing seamounts, island arc basalt and continental fragments which may be of Australian origin. Peak metamorphic conditions, preserved through rapid exhumation, are as high as 2.8 GPa at 550–620°C for the eclogites, but the rocks derived from thicker-crusted seamount and volcanic arc settings were subducted only to lower-P/T blueschist conditions.

ACKNOWLEDGEMENTS

REFERENCES

AUDLEY-CHARLES M. G. 1983. Reconstruction of Gondwanaland. *Nature* **306**, 48–50.

AUDLEY-CHARLES M. G., CARTER D. J. & MILSOM J. 1972. Tectonic development of eastern Indonesia in relation to Gondwana dispersal. *Nature* **239**, 35–9.

BEBOUT G. E., BEBOUT A. E. & GRAHAM C. M. 2007. Cycling of B, Li and LILE (K, Cs, Rb, Ba, Sr) into subduction zones: SIMS evidence from micas in high-*P/T* metasedimentary rocks. *Chemical Geology* **239**, 284–304.

BERGMAN S. C., COFFIELD D. Q., TALBOT J. P. & GARRARD R. A. 1996. Tertiary tectonic and magmatic evolution of western Sulawesi and the Makassar Strait, Indonesia: evidence for a Miocene continent-continent collision. *In* Hall R. and Blundell D. J. (eds.) *Tectonic Evolution of Southeast Asia*. Geological Society of London Special Publication **106**, pp. 391–429

BERRY R. F. & GRADY A. E. 1987. Mesoscopic structures produced by Plio-Pleistocene wrench faulting in South Sulawesi, Indonesia. *Journal of Structural Geology* **9**, 563–71.

CANN J. R. 1970. Rb, Sr, Y, Zr and Nb in some ocean floor basaltic rocks. *Earth and Planetary Science Letters* **10**, 7–11.

CARSWELL D. A., O'BRIEN P. J., WILSON R. J. & ZHAI M. 1997. Thermobarometry of phengite-bearing eclogites in the Dabie Mountains of central China. *Journal of Metamorphic Geology* **15**, 239–52.

CHARLTON T. R. 2000. Tertiary evolution of the Eastern Indonesia Collision Complex. *Journal of Asian Earth Sciences* **18**, 603–31.

COLEMAN R. G., LEE D. E., BEATTY L. B. & BARNNOCK W. W. 1965. Eclogites and eclogites: Their differences and similarities. *Geological Society of America Bulletin* **76**, 483–508.

CONDIE K. C. 1993. Chemical composition and evolution of the upper continental crust: Contrasting results from surface samples and shales. *Chemical Geology* **104**, 1–37.

DEFANT J. M., MAURY C. R., RIPLEY M. E., FEIGENSON D. M. & JACQUES D. 1991. An example of Island-arc petrogenesis: Geochemistry and petrology of the southern Luzon Arc, Phillipines. *Journal of Petrology* **32**, 455–500.

DESPRAIRIES A. & BONNOT-COURTOIS C. 1980. Relation entre la composition des smectites d'altération sous-marine et leur cortège de terres rares. *Earth and Planetary Science Letters* **48**, 124–30.

DROOP G. T. R. 1987. A general equation for estimating Fe^{3+} concentrations in ferromagnesian silicates and oxides from microprobe analyses, using stoichiometric criteria. *Mineralogical Magazine* **51**, 431–35.

ELBURG M. A., VAN LEEUWEN T. M., FODEN J. & MUHARDJO 2002. Origin of geochemical variability by arc-continent collision in the Biru area, southern Sulawesi (Indonesia). *Journal of Petrology* **43**, 581–606.

ESSENE E. J. & FYFE W. S. 1967. Omphacite in Californian metamorphic rocks. *Contributions to Mineralogy and Petrology* **15**, 1–23.

GUNTORO A. 1999. The formation of the Makassar Strait and the separation between SE Kalimantan and SW Sulawesi. *Journal of Asian Earth Sciences* **17**, 79–98.

HAILE N. S. 1978. Reconnaissance paleomagnetic result from Sulawesi, Indonesia, and their bearing on paleogeographic reconstruction. *Tectonophysics* **46**, 77–85.

HALL R. & WILSON M. E. J. 2000. Neogene sutures in eastern Indonesia. *Journal of Asian Earth Sciences* **18**, 787–814.

HAMILTON W. 1979. Tectonics of the Indonesian region. *United States Geological Survey Professional Paper* 1078.

HOLM P. E. 1985. The geochemical fingerprints of different tectonomagmatic environments using hygromagmatophile element abundances of tholeiitic basalts and basaltic andesites. *Chemical Geology* **51**, 303–23.

IRVINE T. N. & BARAGAR W. R. A. 1971. A guide to the chemical classification of the common volcanic rocks. *Canadian Journal of Earth Sciences* **8**, 523–48.

JOHN T., SCHERER E. E., HAASE K. & SCHENK V. 2004. Trace element fractionation during fluid-induced eclogitization in a subducting slab: Trace element and Lu-Hf-Sm-Nd isotope systematics. *Earth and Planetary Science Letters* **227**, 441–56.

KADARUSMAN A., MIYASHITA S., MARUYAMA S., PARKINSON C. D. & ISHIKAWA A. 2004. Petrology, geochemistry and paleogeographic reconstruction of the East Sulawesi Ophiolite, Indonesia. *Tectonophysics* **392**, 55–83.

KATILI J. A. 1978. Past and present geotectonic position of Sulawesi, Indonesia. *Tectonophysics* **45**, 289–322.

KROGH E. J. 1982. Metamorphic evolution deduced from mineral inclusions and compositional zoning in garnet from Norwegian country-rock eclogites. *Lithos* **15**, 305–21.

KULLERUD K., STEPHEN M. B. & ZACHRISSON E. 1990. Pillow lavas as protoliths for eclogites: Evidence from a late Precambrian to Cambrian continental margin, Seve Nappes, Scandinavian Caledonides. *Contributions to Mineralogy and Petrology* **105**, 1–10.

LE BAS M. J., LE MAITRE R. W., STRECKEISEN A. L. & ZANETTIN B. A. 1986. Chemical classification of volcanic rocks based on the total alkali–silica diagram. *Journal of Petrology* **27**, 745–50.

LEAKE B. E., WOOLLEY A. R., ARPS C. E. S. *et al.* 1997. Nomenclature of amphiboles: Report on subcommittee on amphiboles of the International Mineralogical Association, commission on new minerals and mineral names. *Canadian Mineralogist* **35**, 219–46.

LEAKE B. E., WOOLLEY A. R., BIRCH W. D. *et al.* 2003. Nomenclature of amphiboles: Additions and revisions to the International Mineralogical Association's 1997 recommendations. *Canadian Mineralogist* **41**, 1355–62.

LETERRIER J., YUWONO S., SOERIAATMADJA R. & MAURY C. R. 1990. Potassic volcanism in Central Java and South Sulawesi, Indonesia. *Journal of Southeast Asian Earth Sciences* **4**, 171–81.

LUDDEN J. N. & THOMPSON G. 1979. An evaluation of the behavior of the rare earth elements during the weathering of sea-floor basalts. *Earth and Planetary Science Letters* **43**, 85–92.

MARYANTO S., SUSANTO E. E. & SUDIJONO 2004. Sedimentology of Salokalupang formation in Bone Region, South Sulawesi. *Jurnal Sumber Daya Geologi* **1**, 69–83.

MAULANA A. 2009. Petrology, geochemistry and metamorphic evolution of the South Sulawesi basement rocks complexes, Indonesia. M. Phil. Thesis of The Australian National University, Canberra.

MCCULLOCH M. T. & GAMBLE J. A. 1991. Geochemical and geodynamical constraints on subduction zone magmatism. *Earth and Planetary Science Letters* **102**, 358–74.

MESCHEDE M. 1986. A method of discriminating between different types of mid-ocean ridge basalts and continental tholeiites with the Nb–Zr–Y diagram. *Chemical Geology* **56**, 207–18.

METCALFE I. 1998. Paleozoic and Mesozoic Geological Evolution of the SE Asian region: Multidisciplinary constraints and implications for biogeography. *In* Hall R. and Holloway J. D. (eds.) *Biogeography and Geological Evolution of SE Asia*, pp. 25–41, Buckhuys Publishers, Leiden.

MEYER P. S., DICK H. J. B. & THOMPSON G. 1989. Cumulate gabbros from the Southwest Indian Ridge, 54°S-7°16′E: Implication for magmatic process at a slow spreading ridge. *Contributions to Mineralogy and Petrology* **103**, 44–63.

MIYAZAKI K., ZULKARNAIN I., SOPAHELUWAKAN J. & WAKITA K. 1996. Pressure-temperature conditions and retrograde paths of eclogites, garnet–glaucophane rocks and schists from South Sulawesi, Indonesia. *Journal of Metamorphic Geology* **14**, 549–63.

MORIMOTO N., FABRIES J., FERGUSON A. K. *et al.* 1988. Nomenclature of Pyroxenes. *American Mineralogist* **73**, 1123–33.

MORRISON M. A. 1978. The use of 'immobile' trace elements to distinguish the palaeotectonic affinities of metabasites: Applications to the Palaeocene basalts of Mull and Skye, northwest Scotland. *Earth and Planetary Science Letters* **39**, 407–16.

NIU Y. & BATIZA R. 1997. Trace element evidence from seamountsfor recycled oceanic crust in the eastern equatorial Pacific mantle. *Earth and Planetary Science Letters* **148**, 471–84.

PARKINSON C. D. 1996. The origin and significance of metamorphosed tectonic blocks in mélanges: Evidence from Sulawesi, Indonesia. *Terra Nova* 8, 312–23.

PARKINSON, C. D. 1998. An outline of the petrology, structure and age of the Pompangano Schist Complex of central Sulawesi, Indonesia. *The Island Arc* 7, 231–45.

PARKINSON C. D. & KATAYAMA I. 1999. Present day ultrahigh pressure conditions of coesite inclusions in garnet and zircon: Evidence from laser Raman microspectroscopy. *Geology* 27, 979–82.

PARKINSON C. D., MIYAZAKI K., WAKITA K., BARBER A. J. & CARSWELL D. A. 1998. An overview and tectonic synthesis of the very high pressure and associated rocks of Sulawesi, Java and Kalimantan, Indonesia. *Island Arc* 7, 184–200.

PEARCE J. A., BARKER P. F., EDWARDS S. J., PARKINSON I. J. & LEAT P. T. 2000. Geochemistry and tectonic significance of peridotites from the South Sandwich arc-basin system, South Atlantic. *Contributions to Mineralogy and Petrology* 139, 36–53.

PEARCE J. A. & CANN J. R. 1973. Tectonic setting of basic volcanic rocks determined using trace element analyses. *Earth and Planetary Science Letters* 19, 290–300.

PEARCE J. A. & NORRY M. J. 1979. Petrogenetic implications of Ti, Zr, Y, and Nb variations in volcanic rocks. *Contributions to Mineralogy and Petrology* 69, 33–47.

PEARCE N. J. G., PERKINS W. T., WESTGATE J. A. *et al.* 1997. A compilation of new and published major and trace element data for NIST SRM 610 and NIST SRM 612 glass reference materials. *Geostandards Newsletter* 21, 115–44.

PERFIT M. R., GUST D. A., BENCE A. E., ARCULUS R. J. & TAYLOR S. R. 1980. Chemical characteristics of island arc basalts: Implications for mantle sources. *Chemical Geology* 30, 227–56.

POLVÉ M., MAURY R. C., BELLON H. *et al.* 1997. Magmatic evolution of Sulawesi: Constraints on the Cenozoic geodynamic history of the Sundaland active margin. *Tectonophysics* 272, 69–92.

RICKWOOD P. C. 1968. On recasting analyses of garnet into end-members molecules. *Contribution to Mineralogy and Petrology* 18, 175–98.

RYBURN R. J., RAHEIM A. & GREEN D. H. 1976. Determination of the P, T paths of natural eclogites during metamorphism-record of subduction. *Lithos* 9, 161–64.

SASAJIMA S., NISHIMURA S., HIROOKA K., OTOFUJI Y., VAN LEEUWEN T. M. & HEHUWAT F. 1980. Paleomagnetic studies combine with fission-track dating on the Western Arc of Sulawesi, East Indonesia. *Tectonophysics* 64, 163–72.

SASSI R., MAZZOLI C., MILLER C. & KONZETT J. 2004. Geochemistry and metamorphic evolution of the Pohorje Mountain eclogites from the easternmost Austroalpine basement of the Eastern Alps (Northern Slovenia). *Lithos* 78, 235–61.

SAUNDERS A. D. 1984. The rare element characteristic of igneous rocks from the ocean basin. *In* Henderson P. (ed.) *Rare Earth Element Geochemistry*, pp. 205–36, Elsevier, Amsterdam.

SAUNDERS A. D. & TARNEY J. 1984. Geochemical characteristic and tectonic significance of bacK–Arc basin. *In* Kokelaar B. P. and Howels M. F. (eds.) *Marginal Basin Geology; Volcanic and Associated Sedimentary and Tectonic Processes in Modern and Ancient Marginal Basin*. Geological Society of London, Special Publications 16, pp. 59–76.

SHERATON J. W. 1984. Chemical changes associated with high-grademetamorphism of mafic rocks in the East Antarctic Shield. *Chemical Geology* 14, 135–57.

SIMANDJUNTAK T. O., RUSMANA E., SURONO & SUPANDJONO J. B. 1991. *The Geology of the Malili Quadrangle, Sulawesi (Quadrangle 2113), Scale 1: 250,000, 1 Sheet*. Geological Research and Development Centre, Bandung.

SINTON J. M. & FRYER P. 1987. Marian through lavas from 18 degrees N; implication for the origin of back arc basin basalts. *Journal of Geophysical Research* 92, 12782–802.

SORENSEN S. S., GROSSMAN J. N. & PERFIT M. R. 1997. Phengite-hosted LILE enrichment in eclogite and related rocks: Implications for fluid-mediated mass transfer in subduction zones and arc magma genesis. *Journal of Petrology* 38, 3–34.

SPANDLER C. 2004. The Geochemical and petrological evolution of subduction zones: Insight from blueschist to eclogite-facies rocks from New Caledonia and high-pressure hydrothermal experiments. PhD thesis of The Australian National University, Canberra.

SPANDLER C., HERMANN J., ARCULUS R. J. & MAVROGENES J. 2004. Geochemical heterogeneity and element mobility in deeply subducted oceanic crust; insights from high pressure mafic rocks from New Caledonia. *Chemical Geology* 206, 21–42.

SUKAMTO R. 1975. Geological map of Ujung Pandang sheet, scale 1:1,000,000, 1 sheet. Geological Survey of Indonesia.

SUKAMTO R. 1982. Geological map of the Pangkajene and Western part of Watampone, South Sulawesi, scale 1:250.000, 1 sheet. Geological Research and Development Centre, Bandung.

SUKAMTO R. & SUPRIATNA 1982. *Geological Map of Ujung Pandang, Benteng Dan Sinjai, Sulawesi (Quadrangle 2113), Scale 1: 250,000, 1 Sheet*. Geological Research and Development Centre, Bandung.

SUN S. S. & MCDONOUGH W. F. 1989. Chemical and isotopic systematics of oceanic basalts: Implications for mantle composition and processes. *In* Saunders A. D. and Norry M. J. (eds.) *Magmatism in Ocean Basins*. Geological Society of London, Special Publications 42, pp. 313–46.

THOMPSON G. 1973. A geochemical study of the low temperature interaction of sea-water and oceanic igneous rocks. *Transactions of the American Geophysical Union* **54**, 1015–19.

TIEZZI L. J. & SCOTT R. B. 1980. Crystal fractionation in a cumulate gabbro, Mid-Atlantic Ridge, 26°N. *Journal of Geophysical Research* **85**, 5438–54.

TRIBUZIO R., MESSIGA B., VANNUCCI R. & BOTAZZI P. 1996. Rare-earth element redistribution during high-pressure low-temperature metamorphism in ophiolitic Fe-gabbros (Liguria,Northwestern Italy): Implications for light REE mobility in subduction zones. *Geology* **24**, 711–14.

VAN LEEUWEN T. M. 1981. The geology of south-west Sulawesi with special reference to the Biru area. *In* Barber A. J. and Wiryosujono S. (eds.) *Geology and Tectonics of Eastern Indonesia*. Geological Research and Development Centre, Special Publications 2, Bandung, pp. 277–304.

VAN WESTRENEN W., BLUNDY J. D. & WOOD B. J. 2001. High field strength element/rare earth element fractionation during partial melting in the presence of garnet: Implications for identification of mantle heterogeneities. *Geochemistry, Geophysics, Geosystems* **2**, 2000GC000133.

VERMEESCH, P. 2006. Tectonic classification of basalt with classification trees. *Geochimica et Cosmochimica Acta* **70**, 1839–48.

VILLENEUVE M., GUNAWAN W., CORNEE J. J. & VIDAL O. 2002. Geology of the central Sulawesi belt (eastern Indonesia): Constraints for geodynamic models. *International Journal of Earth Sciences* **91**, 524–37.

VROON P. Z., VAN BERGEN M. J. & FORDE E. J. 1996. Pb and Nd isotope constraints on the provenance of tectonically dispersed continental fragments in East Indonesia. *In* Hall R. and Blundell D. J. (eds.) *Tectonic Evolution of Southeast Asia*. Geological Society of London, Special Publications 106, pp. 445–54.

WAKITA K. 2000. Cretaceous acretionary-collision complexes in Central Indonesia. *Journal of Asian Earth Sciences* **18**, 739–49.

WAKITA K., SOPAHELUWAKAN J., MIYAZAKI K. & MUNASRI 1996. Tectonic evolution of the Bantimala Complex, South Sulawesi, Indonesia. *In* Hall R. and Blundell D. J. (eds.) *Tectonic Evolution of Southeast Asia*. Geological Society of London, Special Publications 106, pp. 353–64.

WHITE W. M. 2007. *Geochemistry: An-online Text Book*. Johns Hopkins University Press, Baltimore.

WILSON M. 1989. *Igneous Petrogenesis, A Global Tectonic Approach*. Unwin Hyman, London.

WILSON M. E. J. & BOSENCE D. J. W. 1996. The tertiary evolution of South Sulawesi; a record in Redeposited Carbonates of the Tonasa Limestone Formation. *In* Hall R. and Blundell D. J. (eds.) *Tectonic Evolution of Southeast Asia*. Geological Society of London, Special Publications 106, pp. 365–90.

WINCHESTER J. A. & FLOYD P. A. 1976. Geochemical magma type discrimination: Application to altered and metamorphosed basic igneous rocks. *Earth and Planetary Science Letters* **28**, 459–69.

WOOD D. A. 1980. The application of a Th-Hf-Ta diagram to problems of tectonomagmatic classification and to establishing the nature of crustal contamination of basaltic lavas of the British Tertiary volcanic province. *Earth and Planetary Science Letters* **50**, 11–30.

YUWONO Y. S., MAURY R. C., SOERIA-ATMADJA R. & BELLON H. 1988. Tertiary and Quaternary geodynamic evolution of South Sulawesi: Constraints from the study of volcanic units. *Geologi Indonesia* **13**, 32–48.

ZACK T., RIVERS T. & FOLEY S. F. 2001. Cs-Rb-Ba systematics in phengite and amphibole: An assessment of fluid mobility at 2.0 GPa in eclogites from Trescolmen, Central Alps. *Contributions to Mineralogy and Petrology* **140**, 651–69.

ZHAO Z. F., ZHENG F. Y., CHEN X. R., XIA X. Q. & WU B. Y. 2007. Element mobility in mafic and felsic ultrahigh-pressure metamorphic rocks during continental collision. *Geochimica et Cosmochimica Acta* **71**, 5244–66.